Spring 4-25-2014

EARLY AND LATE IRON DIAGENSIS IN THE UPPER TRIASSIC SHINARUMP MEMBER OF THE CHINLE FORMATION (UTAH AND ARIZONA)

Derek T. Burgess

University of Nebraska-Lincoln, dburgess1@huskers.unl.edu

EARLY AND LATE IRON DIAGENSIS IN THE UPPER TRIASSIC
SHINARUMP MEMBER OF THE CHINLE FORMATION
(UTAH AND ARIZONA)

By

Derek T. Burgess

A THESIS

Presented to the Faculty of

The Graduate College at the University of Nebraska

In Partial Fulfillment of Requirements

For the Degree of Master of Science

Major: Earth and Atmospheric Sciences

Under the Supervision of Professor David B. Loope

Lincoln, Nebraska

May, 2014

EARLY AND LATE IRON DIAGENSIS IN THE UPPER TRIASSIC SHINARUMP MEMBER OF THE CHINLE FORMATION (UTAH AND ARIZONA)

Derek T. Burgess M.S.

University of Nebraska 2014

Advisor: David B. Loope

The fluvial Shinarump Member of the Chinle Formation in southwestern Utah and northwestern Arizona contains several distinct types of diagenetic iron accumulations. They range to more than 50 cm in diameter, and are dominantly composed of iron-oxide cement, but siderite, rhodochrosite and pyrite cements are common. Iron-oxide cements occur in all facies, but are most abundant in channel sandstone bodies. There, iron-oxide-cement occurs as wonderstone fabric (rinds & staining), dispersed rhombic pseudomorphs, and as discoidal concretions within intraformational conglomerates. Evidence from Shinarump sediment indicates that the ferrous carbonate mineral siderite ($FeCO_3$) was the precursor mineral for current iron-oxide cements. Early diagenetic siderite typically forms in environments that are consistently water-logged, organic-rich, sulfate-poor, and methanic. Those environments are typical of freshwater swamps and bogs. It is difficult to find preserved siderite in outcrop because it quickly alters to iron-oxide in oxygenated pore-waters. Rhomb-shaped iron oxide pseudomorphs in sandstones and mm-scale spheroids defined by displaced silt grains within the iron-oxide rinds that surround intraformational clasts indicate pre-existing siderite. Discoidal *septarian concretions* occur in a thinly laminated mudstone facies above channel sands displaying complex fracture networks, iron-oxide cement, and ferrous iron-carbonate cements. *Box-work concretions* are cemented with iron oxide and developed thick rinds along NNW-SSE trending joints. Joint controlled precipitation of iron-oxide indicates early-diagenetic siderite was not oxidized until the onset of Basin and Range deformation (Miocene). *Rinded clasts* are iron-oxide cemented intraformational

mudstone clasts that comprise dense iron-rich rinds surrounding iron-poor centers. Rinds developed after transport of sideritic mud clasts when siderite dissolved and diffusing ferrous iron was oxidized as rinds along fractures inside and along the perimeters of these clasts. Rinds surrounding fractures formed after Basin and Range faulting. *Iron-oxide-cemented clasts* are found in intraformational conglomerates. In thin-section, these pebbles resemble iron-cemented concretions and commonly have sharp edges, suggesting that they represent reworked Shinarump sediments. Box-works, rinded pebbles, cemented channel sands, and septarian concretions indicate that early diagenetic siderite is present.

Table of Contents

SIGNFICANCE OF FE-OXIDE CEMENTATION IN THE SHINARUMP MEMBER

The purpose of this study is to characterize iron-oxide cements within the Shinarump Member and evaluate their relationship to reduced-iron, precursor minerals. These reduced-iron minerals precipitate in only strongly reducing, anoxic conditions associated with methanogenesis and sulfate reduction.

Shinarump Depositional Environment

      i)   Geological Settings

The Shinarump Member of the Chinle Formation was deposited upon an erosional surface in a back-arc basin that formed during the Sonoma orogeny when an island-arc system accreted along the western edge of Pangaea (Dickinson, 1981). The Chinle Basin drainage extended from the craton (western Texas) to the edge of the supercontinent (Arizona, Utah, and Nevada) (Dickinson & Gehrels, 2008). The fluvial Shinarump Member is the lowest stratigraphic unit of the Chinle Formation (Figure 1A), and overlies the Tr-3 Unconformity, which separates the upper Triassic Chinle Formation from the lower Triassic Moenkopi Formation.

The study area (Figures 1B, 2) for this paper is northwestern Arizona and southwestern Utah. Most work was performed in the Chocolate Cliffs near the town of Colorado City, Arizona. The Shinarump Member contains several types of iron-oxide concretions in different localities across the study area. The resistant, cliff-forming Shinarump Member generally decreases in grain size to the northwest. In the study area of this paper, it is composed dominantly of fine to coarse sandstones and locally includes pebble conglomerate. It varies in mineralogical maturity from quartz arenite to quartzose volcanic wacke (Stewart et al., 1972). Conglomerate clasts are mostly extrafromational and dominantly comprise chert, quartz, and quartzite clasts. Iron-oxide clasts are less abundant. Shinarump channel sandstone deposits are cross-stratified, structureless, or horizontally bedded (Stewart et al.,1972; Blakey & Gubitosa, 1983). These fluvial deposits are

Figure 1: (A) Modified stratigraphic column from Dubiel et al.(2011) depicts the Chinle Formation and the stratigraphic relationships over the region. The basal Shinarump Membern (Red) is thin and discontinous as the TR-3 unconformity is deeply eroded into the Moenkopi Formation. The Shinarump fills these paleovalleys. (B) Regional paleogeographic map modified after Dickinson et al. (2008) explaining the regional dispersal direction of the Chinle-Dockum paleodrainage network. The study area is designated by the black box.
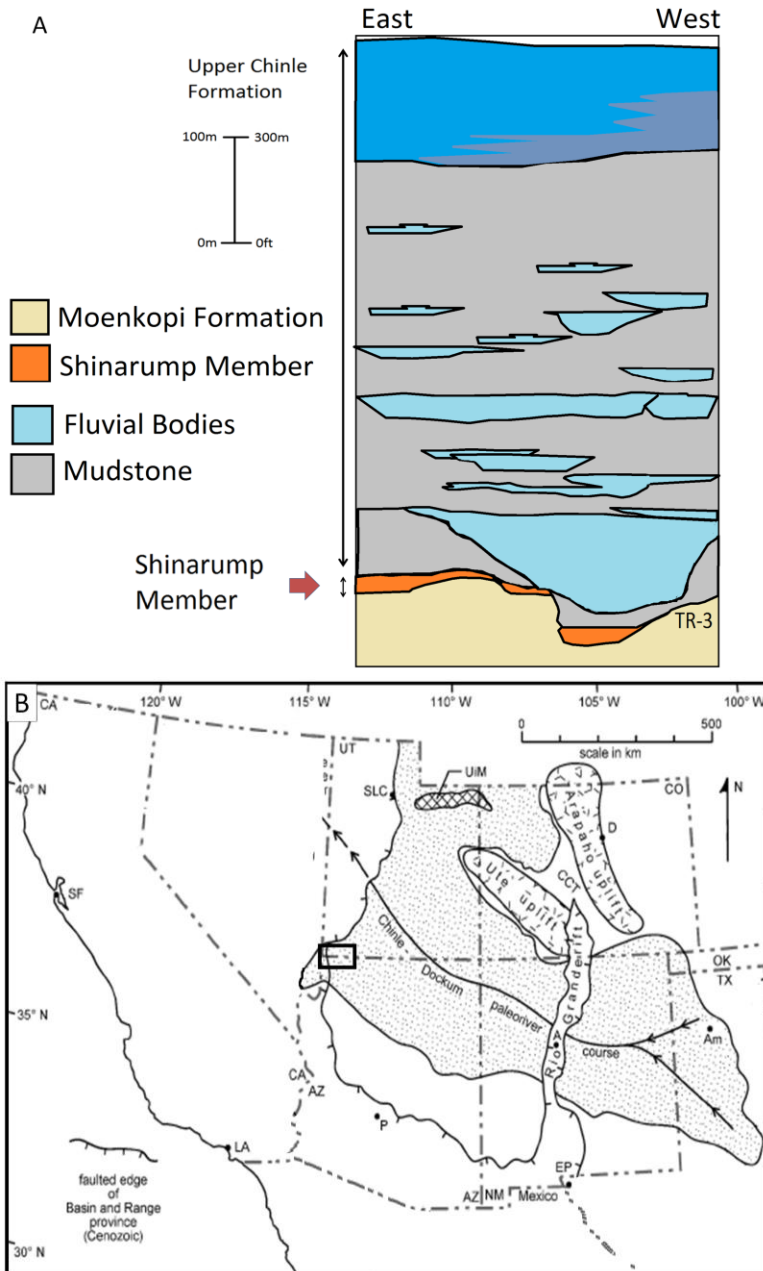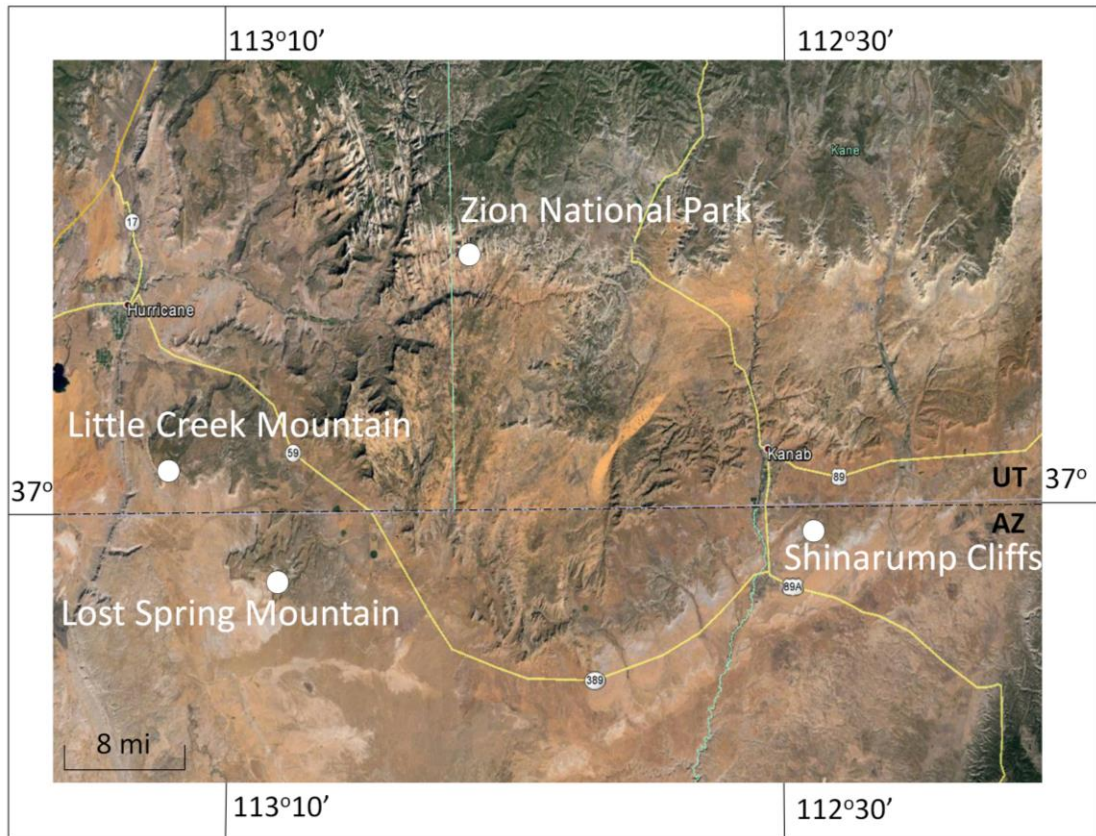
Figure 2: A map showing study sites indicated by white dots.

the initial phase of a transgressive depositional cycle that resulted in the filling of paleovalleys that were deeply incised into the Moenkopi Formation and comprise a low-stand systems tract (Figure 1A) (Beer, 2005). Infilling of deeply incised valleys generated a thin discontinuous sheet

Chinle paleoclimate conditions were controlled largely by the massive size of the Pangaean supercontinent. The nearly equal distribution of landmass across the paleoequator maximized the effects of a monsoon paleoclimate (Peterson, 1988; Kutzbach and Gallimore 1989,; Ziegler et al., 1983; Parrish, 1985). All researchers agree upon a warm paleoclimate, but the amount and distribution of annual precipitation is more contentious (Dubiel et al., 1991). Dubiel recognized that large amounts of precipitation fell annually, but varied seasonally. Ground water tables were therefore consistently high year round. Later, studies of paleosols of the lower Chinle Formation by Prochnow et al. (2006) and Dubiel & Hasiotis. (2011) provided more evidence for this conclusion. The development of oxisols and gleysols during early Chinle deposition suggests humid, water-logged conditions throughout most of the year. Clastic rocks within the Monitor Butte Member (immediately above the Shinarump Member) were deposited in marsh, lake, and delta complexes and also indicate a high water table.

ii) *Reducing Conditions Favorable for Fe-Oxide Precursor Cements*

Low-lying terrestrial deposits containing abundant organic matter lying below the water table are typically anoxic and highly reducing. Reducing pore waters destabilize iron-oxide coatings on sedimentary clastic particles, thereby allowing early diagenetic iron-bearing minerals to precipitate. Pyrite (FeS_2) precipitation is linked to conditions where the presence of sulfate (SO_4^{2-}) in the pore water allows sulphate-reducing microbes to generate hydrogen sulfide (H_2S) (Berner, 1981). Siderite ($FeCO_3$) precipitates in settings wherever the rate of iron reduction exceeds sulphate reduction (Pye et al., 1990). Pye and Berner attribute the precipitation of most
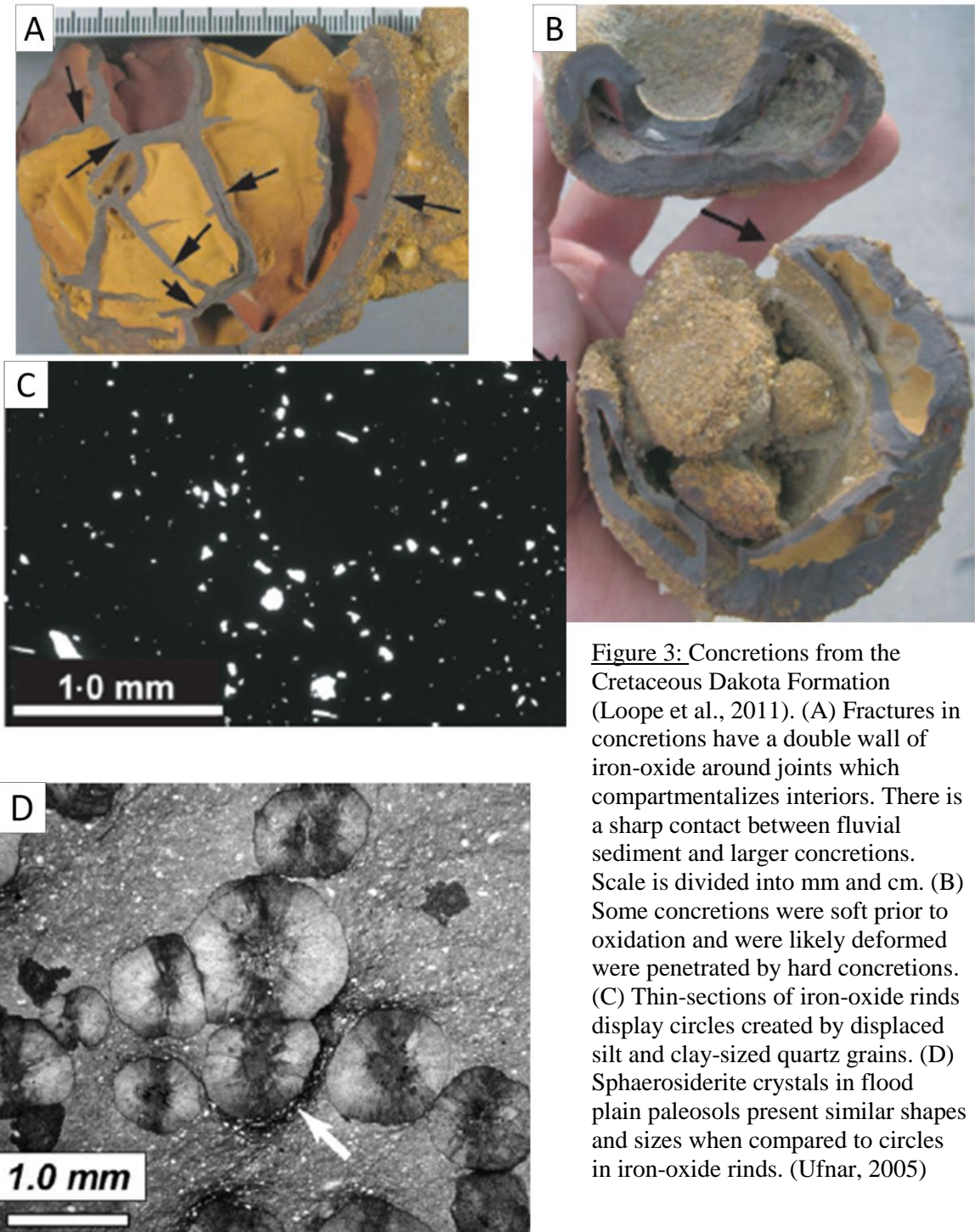
Figure 3: Concretions from the Cretaceous Dakota Formation (Loope et al., 2011). (A) Fractures in concretions have a double wall of iron-oxide around joints which compartmentalizes interiors. There is a sharp contact between fluvial sediment and larger concretions. Scale is divided into mm and cm. (B) Some concretions were soft prior to oxidation and were likely deformed were penetrated by hard concretions. (C) Thin-sections of iron-oxide rinds display circles created by displaced silt and clay-sized quartz grains. (D) Sphaerosiderite crystals in flood plain paleosols present similar shapes and sizes when compared to circles in iron-oxide rinds. (Ufnar, 2005)

reduced iron-carbonate minerals (especially siderite) to terrestrial environments with low concentrations of sulphate. It is uncommon for pyrite to co-precipitate with siderite because H_2S readily combines with iron to precipitate pyrite. Where they do form together it is likely that they precluded or preceded one another as redox conditions changed. In conditions where sulphate reduction is absent or outpaced by iron reduction, siderite and other ferroan carbonates can precipitate. Mudstones in floodplain environments, like those along the lower Mississippi River often contain siderite (Ho, C. and Coleman, J.M., 1969). Siderite (Figure 3D) in floodplain paleosols can precipitate as distinct, mm-scale spheroids with a radial crystal structure (sphaerosiderite). Sphaerosiderite has delta^{18}O values that are in equilibrium with local meteoric water (Ludvigson et al., 1998). Sphaerosiderite crystals not only contain useful isotopic data, but their distinct spheroidal shape is easy to identify petrographically. Siderite is often overlooked (Berner, 1981) because it is hard to differentiate between non-reduced and reduced-carbonate minerals under a normal transmitted-light microscope. Identification often requires analysis by a microprobe or other chemical methods.

Concretions and Concretionary Cements

  i)   Concretionary Cements

  A number of minerals form cements in a wide variety of concretions (Mozley, 1989; Pratt, 2001; Melezhik et al., 2007). The most intensely studied concretions are those cemented by carbonate minerals, but pyrite, iron oxides, and other cements are also common (Mozley, 1996). The conventional model describes concretion growth as even and radial, with chemical variations from center to edge. The pervasive model of Mozley. (1989) describes tiny individual nucleation sites across the concretion. Spheres grow simultaneously and each individual sphere records pore-water chemistry changes from center to edge. Variations in cement chemical composition reflect the changes in pore water chemistry during concretion growth.
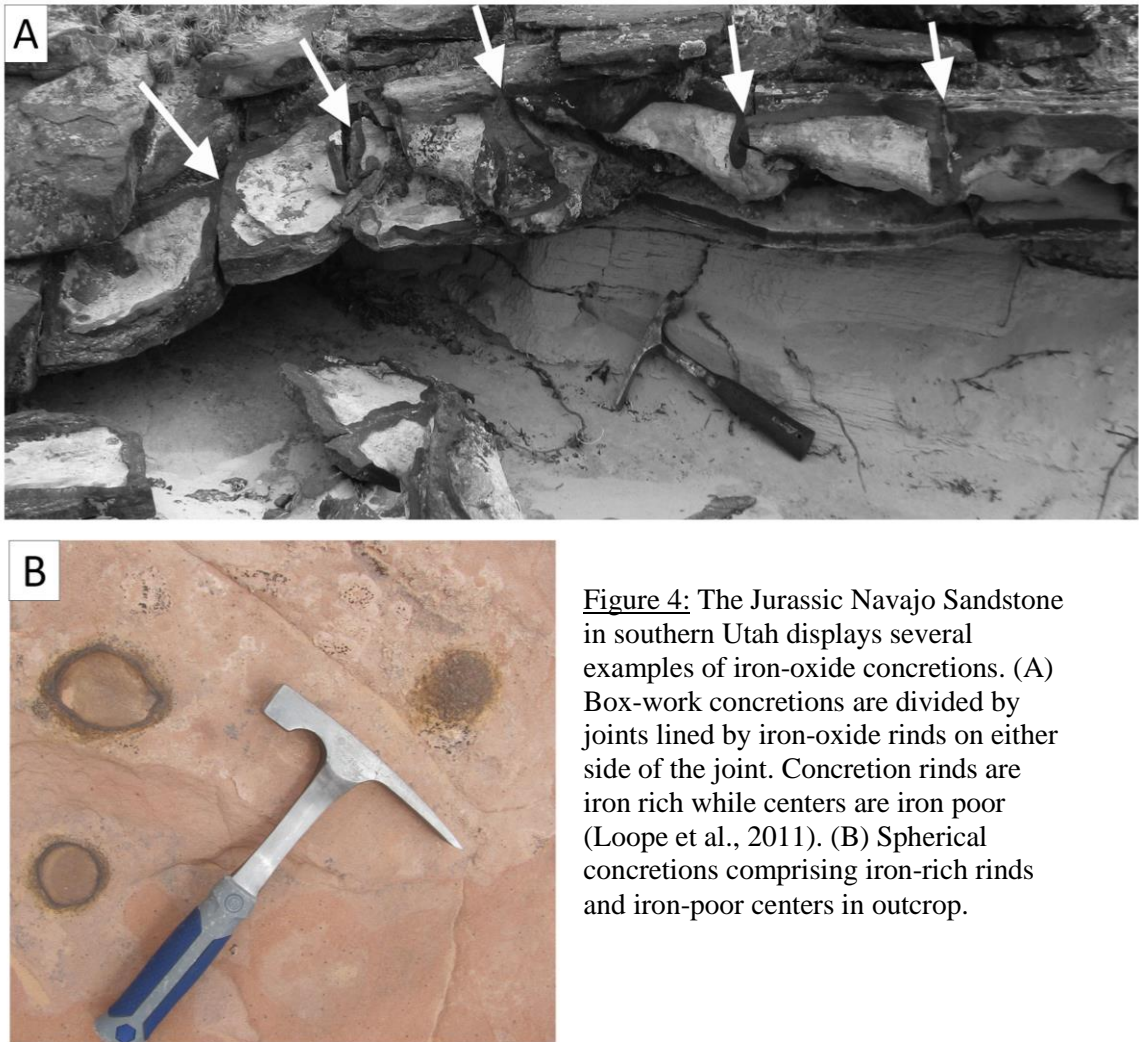
Figure 4: The Jurassic Navajo Sandstone in southern Utah displays several examples of iron-oxide concretions. (A) Box-work concretions are divided by joints lined by iron-oxide rinds on either side of the joint. Concretion rinds are iron rich while centers are iron poor (Loope et al., 2011). (B) Spherical concretions comprising iron-rich rinds and iron-poor centers in outcrop.

The cements themselves can seal off interior sediments and cements from outside pore water and prevent alteration caused by changing groundwater chemistry. Because sediments compact during burial, the approximate depth of concretion formation, in terms of shallow or deep, can be inferred from the amount of intergranular space and by cross-sectional shape.

      ii)   Previously Studied Concretions

Early diagenetic minerals are subject to alteration if ground water chemistry changes. Reduced-iron minerals are unstable in oxygen-rich conditions, and oxidize, producing secondary minerals (Curtis and Coleman, 1986). Recognizing these secondary minerals and linking their presence to the oxidation of a precursor mineral are essential to understanding the evolution of pore-water chemistry. Iron-oxide concretions of the Jurassic Navajo Sandstone have been identified as products of changing redox conditions during late diagenesis (Loope et al., 2010, 2011; Kettler et al., 2012). The Navajo Sandstone of south-central Utah contains iron-oxide cementation that forms box-works (Figure 4A), pipes, and spheroids (Figure 4B). Eolian environments are often very oxic, and mobilization of reduced iron during deposition or at an early stage in diagenesis is unlikely because little organic matter is present. In the Navajo Sandstone, late diagenetic, reducing pore-water flowed through anticlines charged with CO_2 and CH_4 and mobilized iron from iron-oxide coatings on quartz grains (Beitler et al., 2003; Loope et al., 2010). Groundwater flowed down gradient from anticlines and precipitated siderite in concretions of varied shapes and sizes. Although no siderite has been found in Navajo concretions, several lines of evidence point towards siderite as the precursor cement for the abundant iron-oxide accumulations. Box-work concretions have dense core stones cemented with iron oxide and are surrounded by friable sandstone moats. Rhomb-shaped pseudomorphs composed of iron oxide are abundant in core stones. Core stones indicate a central source of iron in the concretion while friable sand indicates that iron cement was dissolved and migrated to form
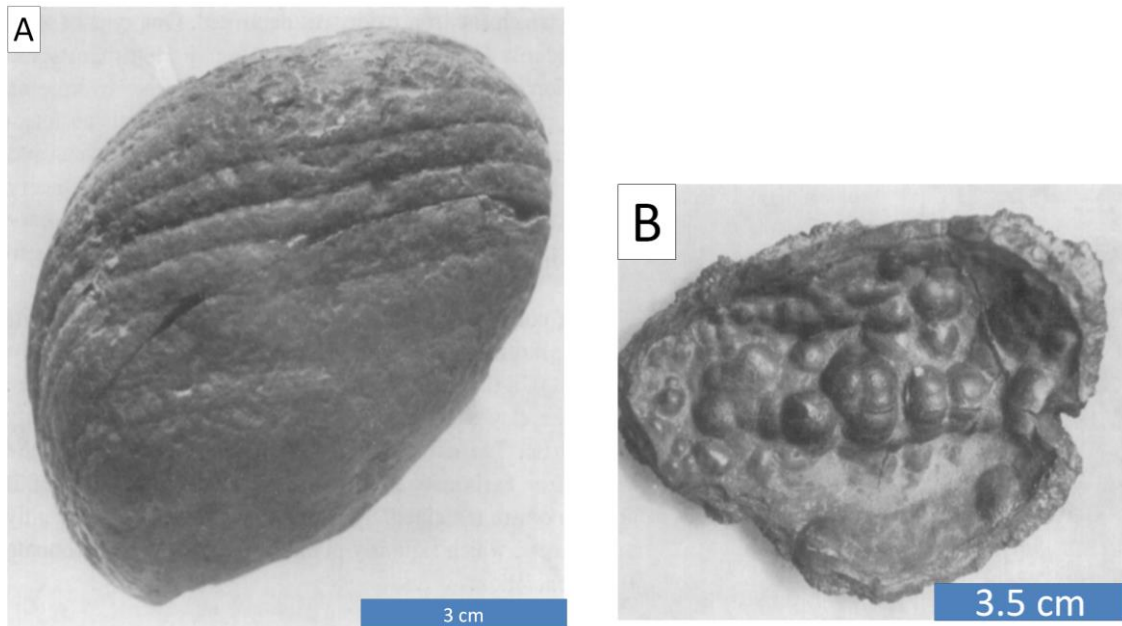
Figure 5: Photographs A & C from Van den burg (1969) and B from Van den burg (1970) are analogous to Shinarump rinded concretions as they share many similar features. (A) Bedding planes are preserved by iron-oxide cementation. (B) Rinds display a botryoidal texture of iron-oxide-cemented sediment. (C) is a siderite concretion with desiccation cracks (a) and depressions on the concretion (b).
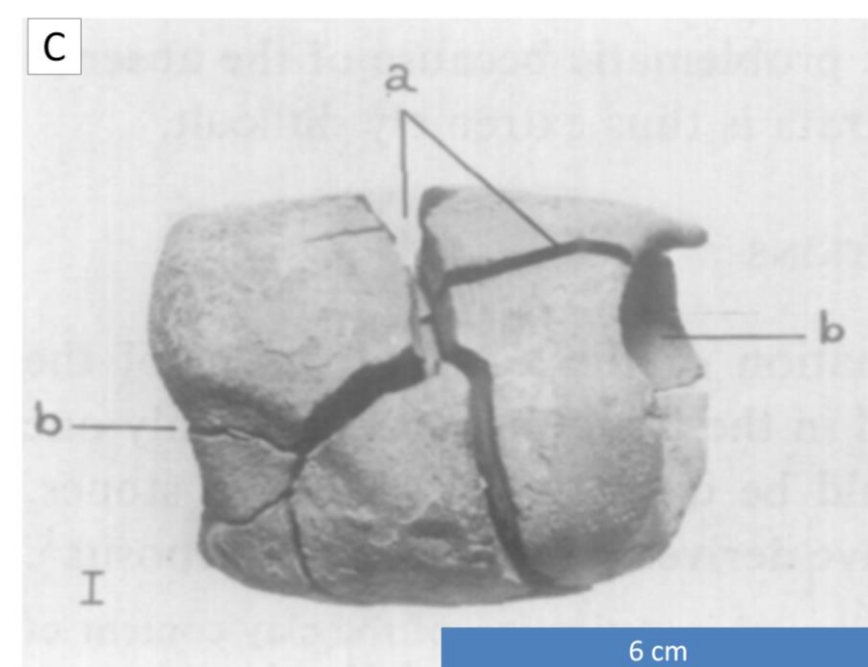
iron-oxide-rinds (Loope et al., 2011). Euhedral carbonate minerals include ferroan calcite, ankerite, and siderite. Mass balance calculations based on the percentage of spheroidal concretion volume and the percentage of iron oxide found in rinds favors siderite as the original (precursor) cement (Loope et al., 2010).

Van der Burg. (1969, 1970) studied rinded mud clasts in fluvial Pleistocene sand and gravel deposits of the Netherlands. Rattle stones (Figure 5 A, B, and C), as they are referred to, have clay centers and a laminated, iron- oxide outer rind. Iron-oxide rinds develop in the outermost portions of the mud clasts and grow inward, cementing the mudstone exterior. Mudstone either fills the concretion interior, or a portion is occupied by void space cause by cement loss. Rattle stones have different shapes and textures that are formed during transport and oxidation processes .Van der burg. (1969, 1970) found rattle stones to be products of oxidized siderite because siderite cement was found in some concretion interiors. Dutch Pleistocene concretions are allochthonous, and can be considered intraformational clasts. Siderite-cemented mudstone originated from floodplain deposits. Flood plain paleosols were entrained in fluvial systems via erosion, transported short distances prior to being deposited, and they were later oxidized.

Loope et al. (2012) described similar allochthonous iron-oxide-concretions (Figure 3A &3 B) from the Cretaceous Dakota Formation in southeastern Nebraska. The Dakota Formation was deposited along the eastern margin of the Western Interior Seaway. Concretions in Dakota basal lag deposits are analogous to allochthonous concretions described by Van der Burg (1969). Early diagenetic siderite is present within subsurface paleosols as sphaerosiderite (Figure 3D) crystals and as rhombic cement in channel sandstones (Ludvigson, 1998). In some cases, thin-sections show rhombic goethite cement as the result of likely oxidized siderite (Ludvigson, 1996). Dakota rattle stones display evidence for a pedogenic origin because of clay centers, iron-

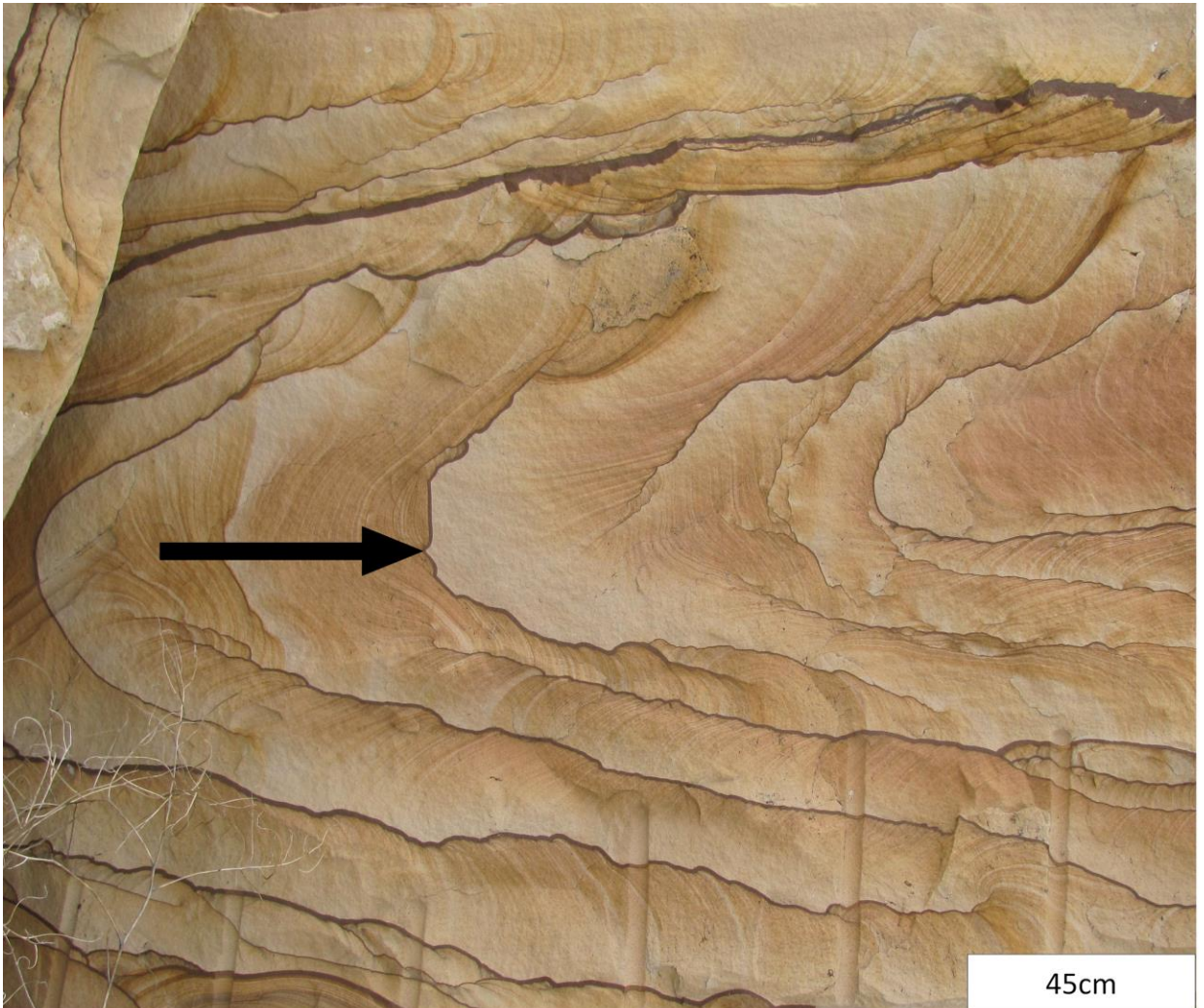Figure 6: Photograph of a Shinarump outcrop displays the wonderstone cementation pattern. Wonderstone consists of alternating iron-oxide rinds and iron-oxide cementation. Rinds and staining are orientated in a consistent direction. The convex side of cuspate surfaces on the iron staining and iron cementation shows the direction of cementation progression. The black arrow indicates the direction of progress.

cemented root traces, and spheroidal outlines formed by quartz particles likely produced by displacive growth of sphaerosiderite crystals (Figure 3C) (Loope et al., 2012).

Kettler et al. (2012) has studied the iron-oxide cementation pattern locally called wonderstone (Figure 6). Wonderstone is found in the channel sandstone facies of the Shinarump Member in southwestern Utah and northwestern Arizona. The wonderstone fabric is the combination of iron-oxide staining and iron-oxide-cement. Sinuous bands of iron-oxide cement alternate with bands of iron-oxide staining. The area between cement bands regularly varies between lightly stained rock and rock lacking iron-oxide staining (Kettler et al., 2012). Many of the bands of iron-oxide staining are arcuate and appear to be truncated by the bands of iron-oxide cement. Both cement and staining conceal sedimentary structures and are related spatially to vertical joints that cut the sandstone at regular intervals. Kettler et al. (2012) have identified the phenomenon between the individual cement bands to be Liesegang banding according to the Jablczynski spacing law. Wonderstone therefore is a combination of both iron-oxide cement bands and iron-oxide staining. Thick arcuate bands mark previously stable boundaries within siderite-cemented sandstone where microbes controlled redox fronts. Iron staining represents a loss of control during rapidly changing redox boundaries that worked inwards toward a central source of iron.

Septarian concretions are common and are produced by calcite and siderite cementation in mudrocks of marine, marginal-marine, and lacustrine environments (Pratt, 2001, Hendry, 2006, Melezhik, 2007). Although septarian concretions receive attention for their complex fracture networks and alternating crack cements that create desired pieces of art, they are poorly understood. There is little dispute over the timing of concretion formation, but for septarian cracks, multiple proposed theories compete regarding their origins, generations, sizes, shapes, and internal stresses. The most common types of cracks are dehydration, shrinkage, or tensional
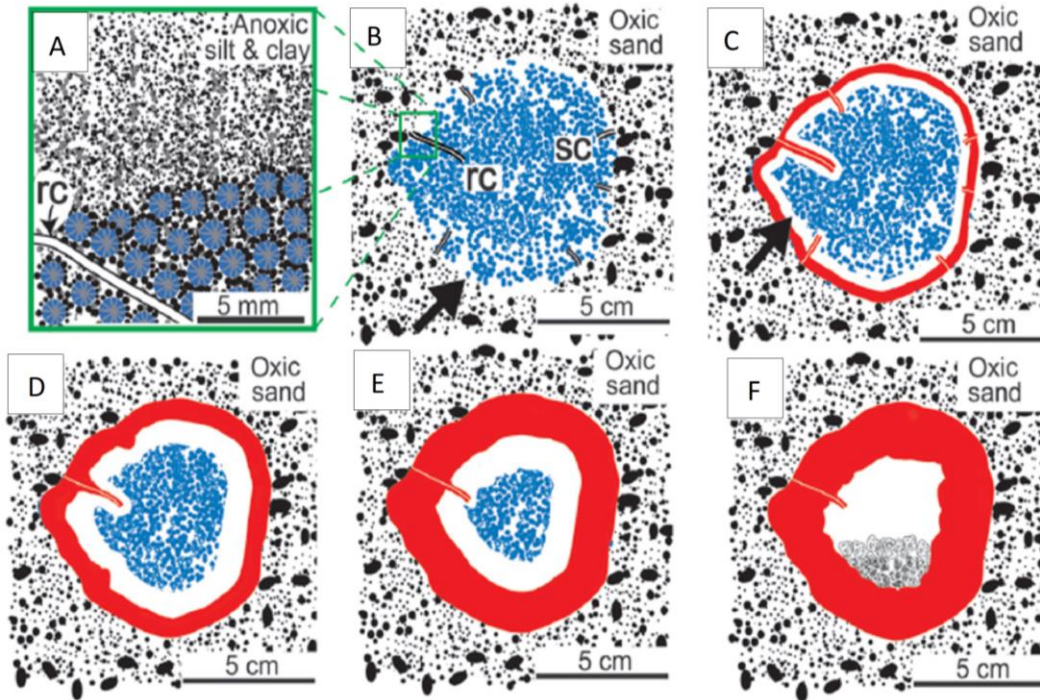
Figure 7: Diagram illustrating the oxidation of a siderite-cemented mudstone clast and the formation of a rattle stone concretion from the Cretaceous Dakota Formation (from Loope et al., 2012). 'rc" indicates root channels and 'sc' indicates shrinkage cracks. (A) Siderite (Blue) bearing sediments are highly reducing. When those conditions change and become oxidizing (B), reduced iron is released from dissolving siderite and diffuses toward a redox front where it is oxidized, forming an iron-oxide rind (C). Persisting oxidizing conditions (D-E) lead to the eventual demise of siderite (F). Microbes often catalyze these reactions. Taking advantage of electron transfers between iron species (ferric (Fe^{+3}) to ferrous (Fe^{+2}) iron), microbes stabilize the redox front (C-F). Evidence of iron-oxidizing microbes have been found on the inner surfaces of similar rinded concretions in the Navajo Sandstone (Weber et al., 2012).

cracks (Pratt, 2001). Shrinkage cracks are wide; vary in size, and orientation. It is easy to identity them, but fitting the opposing sides back together is difficult. In some cases, a large gap persists, and it is often filled with calcite cement. Tensional cracks are very thin compared to dehydration or shrinkage cracks and have little displacement.

iii)   Microbial Oxidation of Siderite Cements

Many reactions on Earth are catalyzed by microbes. Under conditions where light, organic carbon, and oxygen are absent or in short supply, iron oxidizing microbes can use ferrous iron as an energy source. This process has been applied in the interpretation of the concretions of the Navajo Sandstone by Weber et al. (2012). Weber et al. (2012) noted that ferrous iron (FeII) is in short supply in oxidizing environmental conditions, but in highly reducing conditions, like the late diagenetic environment modeled for the Navajo Sandstone, an abundant supply of ferrous iron (FeII) became available. It was proposed that the reduced iron-carbonate minerals such as siderite or ankerite could be used as an energy source and a source of inorganic carbon for microbial metabolic activities. During oxidation in low oxygen conditions, siderite dissolves and iron becomes mobile in its reduced state. Siderite dissolves because the net reaction produces excess acid and is therefore self-promoting (Loope et al., 2011). Microbes are able to stabilize redox fronts and manage the supply of iron and oxygen (Weber et al., 2012). When O_2 is in limited supply, (FeII) metabolizing microbes process the FeII faster than it can be oxidized abiotically, so microbes control the redox reactions at the concretion boundaries. Microbes successfully metabolize iron dissolving from iron carbonate minerals within the concretions and rinds are formed (Figure 7A-F). Oxidation can occur in an abiotic setting when O_2 reaches a critical level. At that threshold, these microbes no longer can control the redox front and oxidation begins to occur abiotically.
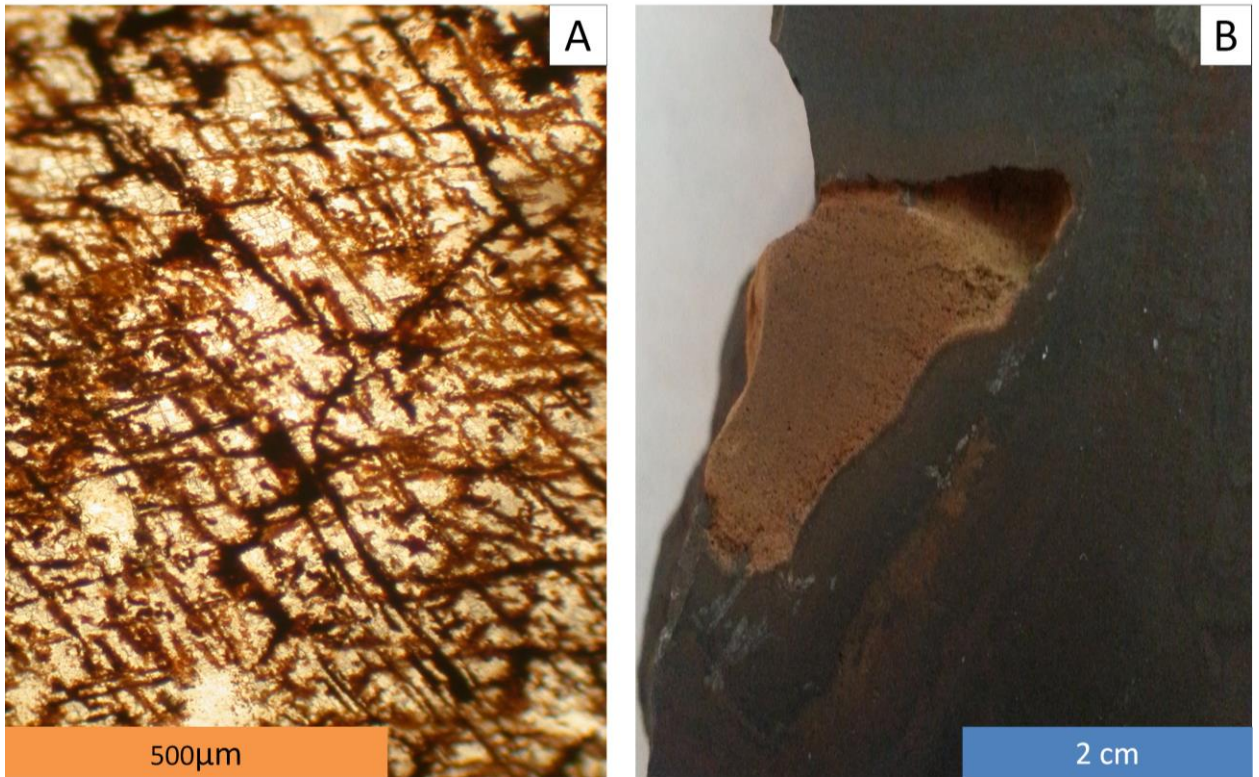
Figure 8: (A) Rhombic cleavage planes are commonly associated with Fe/Mn carbonate minerals. Thin sections from discoidal concretions reveal iron-bearing carbonate minerals with opaque-oxide defining cleavage planes. (B) Faintly bedded, friable, iron poor core stones in septarian concretion interiors.

Mineral Name	Area%		Mineral Name	Area%
Calcite_AMRC	10.27		Phosphates	0.23
Ca/Mg Carbonate	0.02		Ti Minerals	3.91
Fe Carbonate (Siderite)	20.93		Pyrite	3.07
Fe/Mn Carbonate	12.43		Fe-ox/hydro-silicate	3.23
Mn/Fe Carbonate	12.91		Fe Phase	1.33
Silicates	8.36		Mn Phase	2.97
Barite	19.08		other minerals	1.16
			Others	0.10
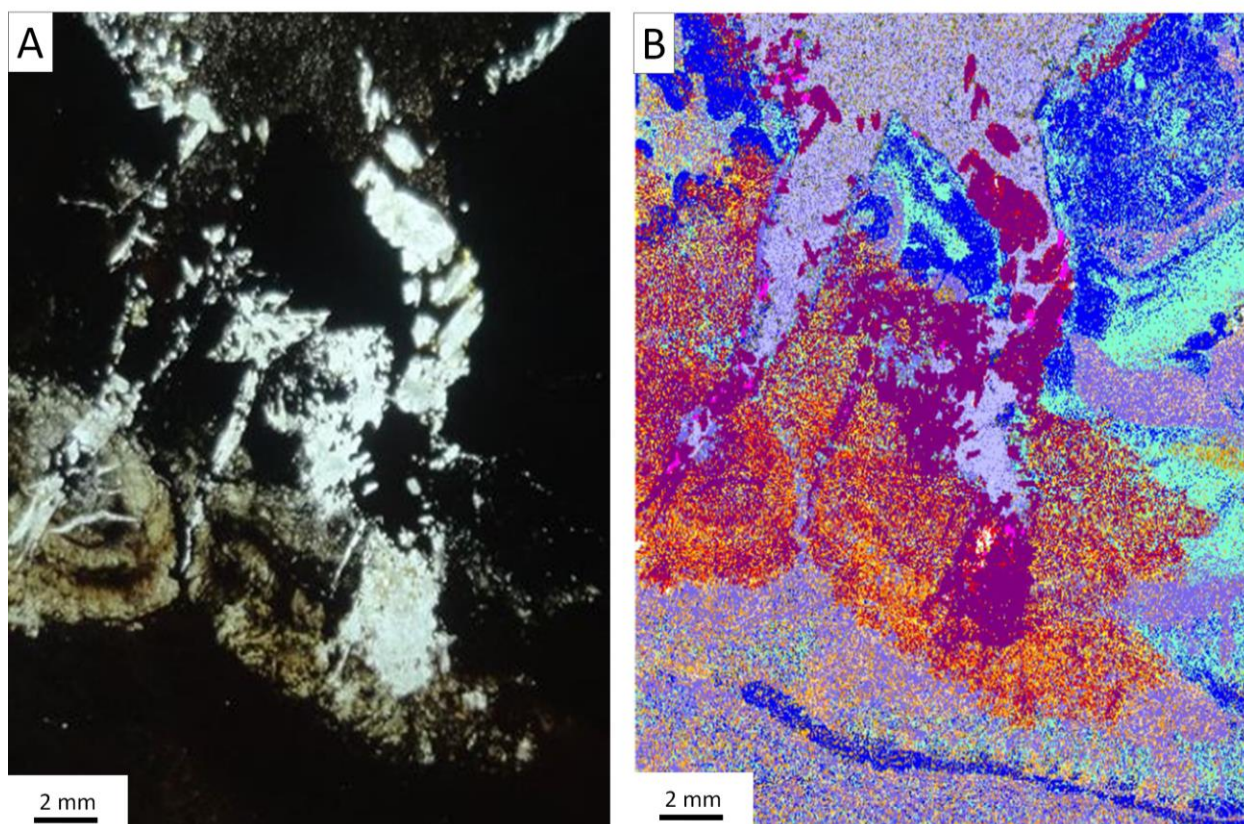
Figure 9: A thin section from a large septarian concretion (A) was subjected to microprobe analysis (QemScan). The analysis produced (B) a map of the mineral distribution across the thin section. The legend displays percent area per mineral. A large percentage of the thin section comprises reduced iron minerals (> 45%). Most of the concretion is opaque despite the changes in mineralogy. This is likely due to continuing oxidation of reduced iron minerals. Barite (white in A, purple in B) is highly visible beside the opaque iron oxide cement.
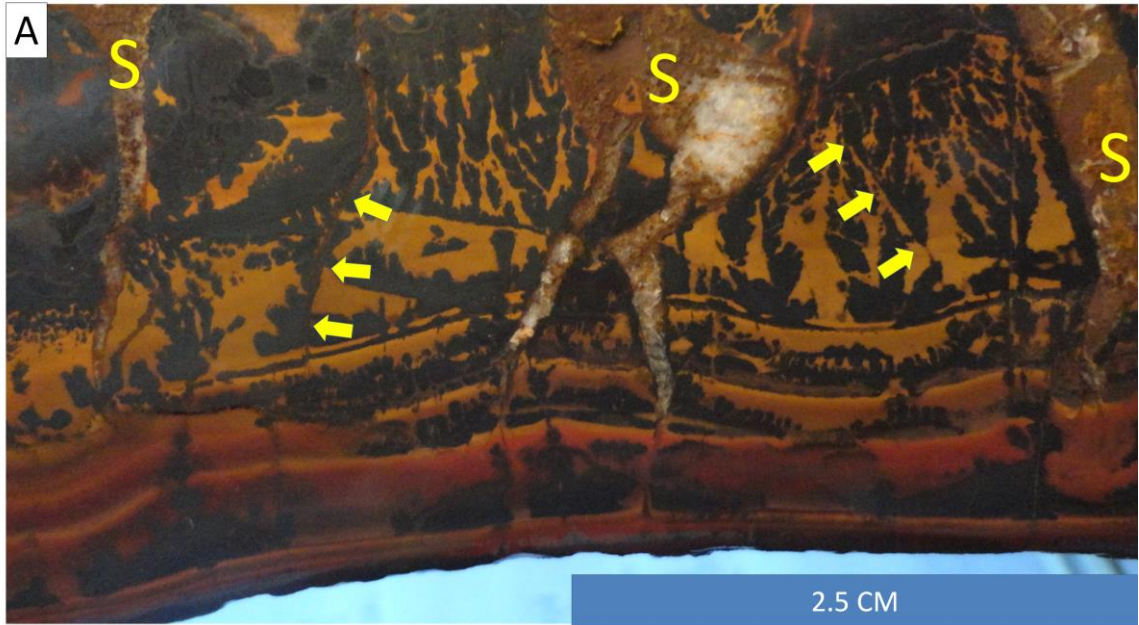
Figure 10: Septarian concretions display many distinctive physical characteristics. Photograph (A) displays septaria (S), hairline fracture (yellow arrows), dendrites and iron banding. These surfaces commonly facilitate different kinds of cementation. Dendrites originate along fractures and bands and grow toward. Large septarian concretions (B) are found outcropping in a thinly laminated mudstone at Little Creek Mountain. Reflected light photomicrograph (C) of pyrite from a septarian concretion shows signs of oxidation (dark grey) within the darker portion of the pyrite crystal.
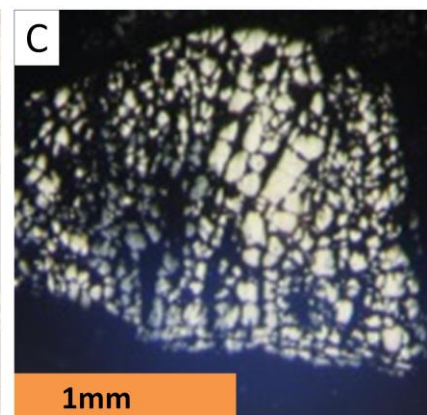
FACIES ANALYSIS

Iron-oxide-cements and concretions were found in multiple facies in the Upper Triassic Shinarump Member of the Chinle Formation. The following section presents the different depositional facies seen at Shinarump outcrops and describes and interprets the different concretions and cements that were found in each.

Thinly Laminated Mudstone Facies

     i)   *Discoidal Concretions*

          a. Description

A thinly laminated mud unit directly overlies a current-rippled sandstone surface near the top of the Shinarump Member at Little Creek Mountain. The mud unit forms a gentle recessive slope between two sandstone units. Intact, large septarian concretions are found in outcrop (Figure 8B) and centimeter-scale shards of shattered concretions litter the slope. Discoidal concretions vary in size, the largest being over 50 centimeters in greatest diameter, with a mass of approximately 55 kg. Host material is composed mostly of silt to clay-sized grains. Bedding is faintly visible in some concretions and, in some cases, overprinted with iron-oxide cement. Concretion centers contain the best examples of faintly bedded siltstone, (Figure 9B) because they are often devoid of any significant cementation.

Intact concretions are zoned and diversely cemented. Cement (Figure 10B) is chiefly found as reduced-carbonate minerals which include siderite (Figure 9A), rhodochrosite and other reduced carbonate phases (46%), barite (20%), calcite (10%), and minor amounts of iron oxide (4%), and pyrite cement (3%) (Figure 8C). These values were determined using QemScan at Colorado school of Mines, a technique where a map of mineral distribution is generated using a microprobe. Cementation and cracking is prevalent throughout the concretions. Septarian cracks

are almost always filled by calcite. Barite is restricted to fracture fills and appears to replace calcite crystals within septarian fractures.

Septaria vary widely in size and shape. Some have very wide cracks filled with calcite cement and / or sediment, while others are very thin and lack both. It is rare for there to be a combination of both crack types, but it is common to find sediment fills together with septaria cements. Some wide cracks are arranged in a radial fashion, whereas many thin cracks occur in orthogonal sets. Fractures that terminate at concretion edges control cementation; whereas internal fractures do not. Cracks penetrating concretion edges are open conduits to the concretion exterior. There are multiple fracture sets as they cross cut one another. Septaria both control and cross cut other cements. Dendrite cements (Figure 8A), for example, start along edges and fill outward. Edges include fractures, but also include concentric bands around concretion exteriors (which likely acted as a hardened surface during cement precipitation). Septaria control dendrites and laminated iron banding. Most cracks in the observed concretions predate cementation, but a few crosscut cementation, banding, and other cracks. Some cracks are restricted to areas of only certain cements. It is clear that multiple stages of cracks and cementation are needed to fully explain the history of these concretions.

> b. *Interpretation*

Large discoidal concretions that are found in the thinly laminated mud unit are cemented primarily by reduced carbonate minerals. Concretion formation in the mudstone likely started early (as are most septarian concretions), but fracturing and fracture filling continued with burial. The first cements formed under highly reducing conditions. Rhodochrosite typically forms

Figure 11: (A) Box work concretions in current rippled sandstone facies. Dense iron-oxide-rich rinds are found along joints. Core stones are found between iron- rich rinds in this example. (B) The interior of a box work concretion is weathered with iron-poor sediment eroded away. When exposed for long periods of time, core stones weather leaving only iron-oxide-rich rinds behind. (C) At Little Creek Mountain, 175 joint orientations were measured. The prominent strike direction is 173°-353° similar to other joints in the study area.

Little Creek Mtn.

N=175
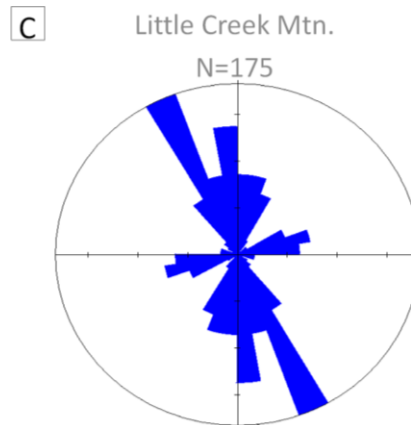
Figure 12: (A) Box-work concretions have formed in the current-rippled sandstone unit at Little Creek Mountain. Joints are bounded on each side with a double wall of iron oxide. Centered in these rinds are iron-poor (relative to rinds) centers. Fractures in box-work concretions are parallel to larger scale structural joints. Weathered pyrite concretion (white arrow) predates jointing and oxidation. Pyrite concretions weather differently than the minerals forming box-work concretions.
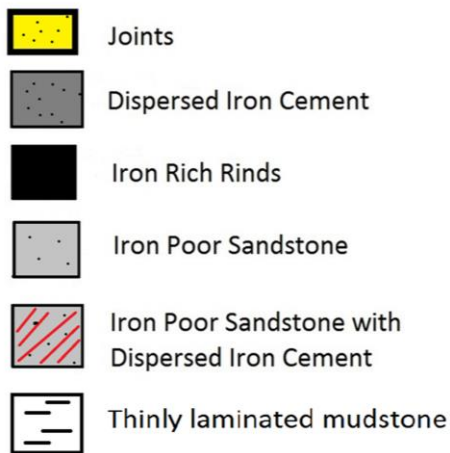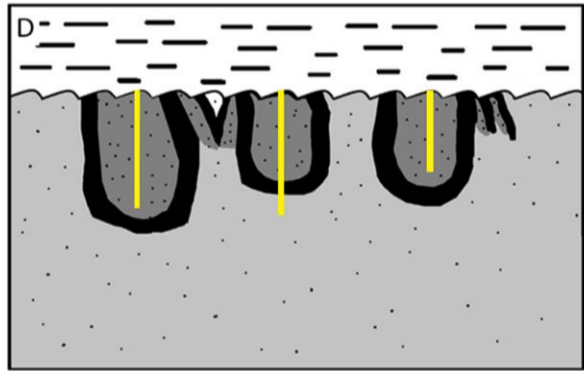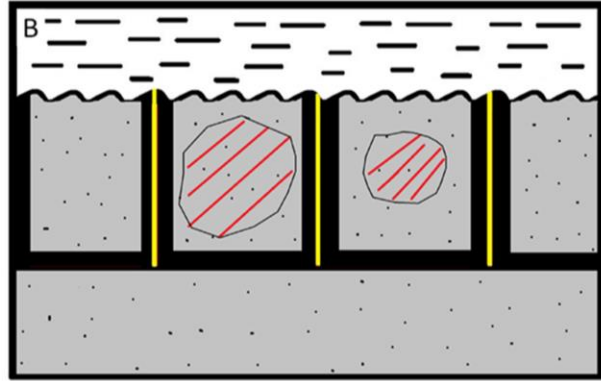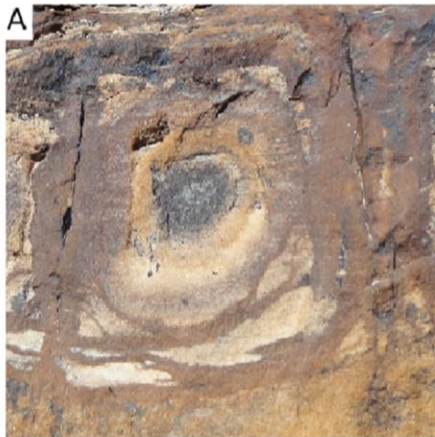
Figure 13: (A) Shinarump box work concretions develop at the contact between the laminated mudstone and current ripple laminated sandstone. Typical box-work concretions form with a double wall of iron-oxide around the joints and iron poor centers. When microbe-controlled redox fronts become unstable, core stones form abiotically. (B) The hypothetical cross-section based on typical box-work concretions in outcrop explains how concretions are arranged. (C) Slabbed cross-section of horseshoe-shaped concretions. These concretions have dispersed iron-oxide cement that lies between rinds and joint. Abiotic oxidation took place before microbes stabilized redox fronts, leading to the dispersed iron-oxide cement around joints. Rinds take the shape of horseshoes and rinds thicken outwards towards the source of iron. Oxygen-rich waters are supplied via the joints. (D) A hypothetical cross-section of a contact bears horseshoe-shaped concretions

dendrites, and iron-oxide dendrites can be found originating from cracks in the concretions. Dendrites have the shape of branching shrubs. Fractures can be found in the tips of these shrub-like cements indicating fracturing after cementation. The most obvious cements that post-date fracture formation are calcite and barite. These cements fill voids left behind after fracture formation. But some barite has replaced calcite crystals in the fracture fills. This change in chemistry from a strongly reducing to a more oxidizing system is seen in the types of cements seen in septarian concretions. The bulk of the concretions are composed of reduced carbonate minerals and oxidation is very late (see below) and is currently taking place. The thinly laminated mud unit likely protected many of the large concretions from oxidizing waters as it is highly impermeable.

Iron-Oxide-Cemented *Channel Sandstone Facies*

i) *Box-work concretions*

      a. *Box-Shaped concretions*
         i. *Description*

Iron cements around fractures in current rippled sandstones at Little Creek Mountain create concretions similar to the box-work concretions described by Loope et al. (2011) in the Jurassic Navajo Sandstone (Figure 4A). At Little Creek Mountain, two forms of box-work concretions have been observed within the uppermost current-rippled sandstone facies (Figure 11A), just below its contact with the laminated mudstone facies.

In outcrop, two or more sets of joints form the boundaries between adjacent concretions (Figure 12A). Joints are contoured on the inside by rinded-iron-oxide cement (Figure 13A). The mean resultant direction of 175 measured joints is 173° / 353° (Figure 11C). Box work concretion centers are iron poor in comparison to rinds. Interiors of concretions are frequently protected by the enclosing rinds of iron cement, but, when the exterior rinds are gone, interiors
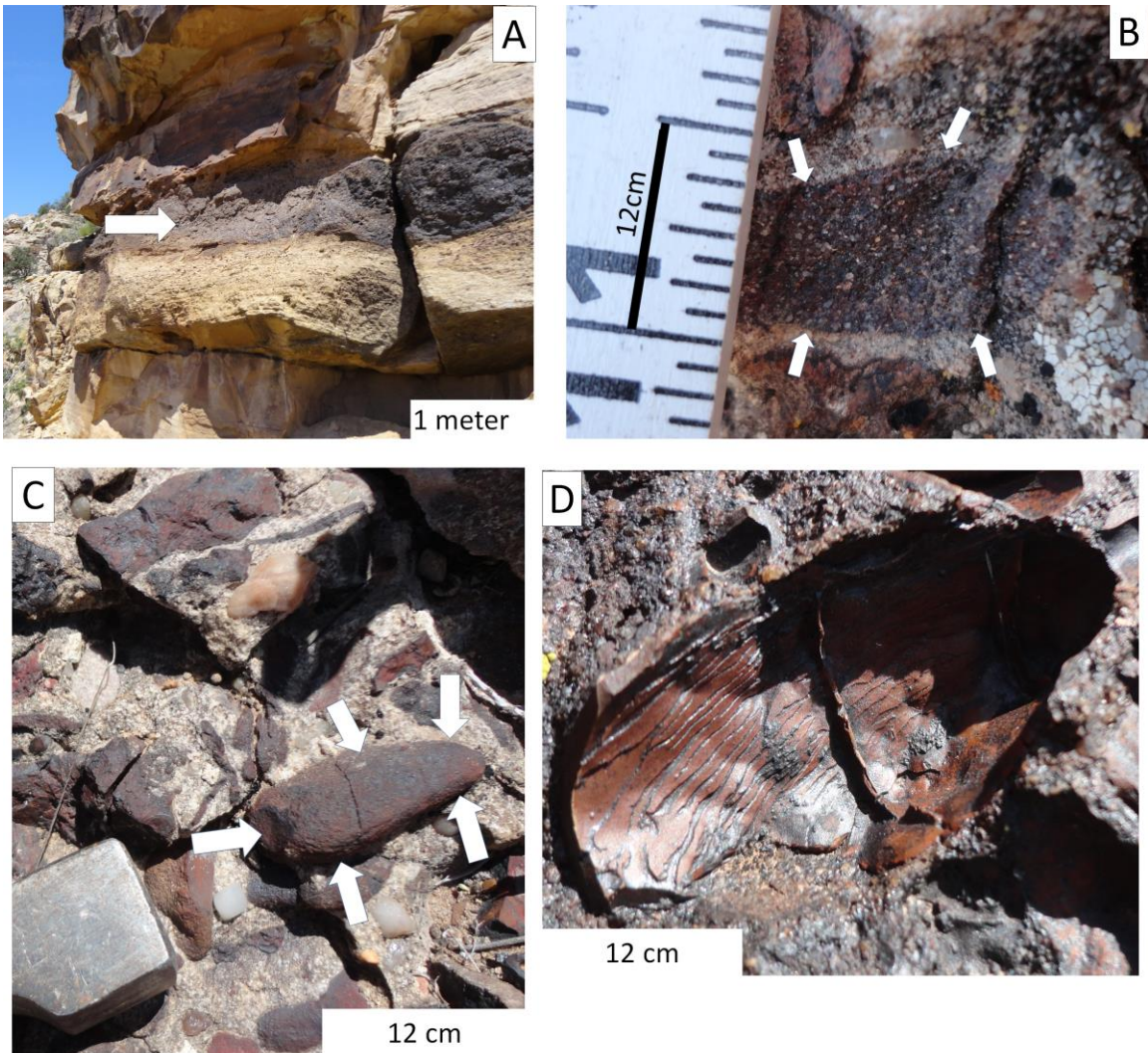
Figure 14: (A) An iron-rich intraformational lag deposit contains a variety of iron-oxide-cemented clasts displayed in illustrations (B, C, and D). (B) An example of reworked iron-oxide-cemented sandstone has no preferential oxidation that forms rinds. Iron cement is evenly distributed through the clast. (C) Reworked mudstone clasts are evenly cemented by iron-oxide cements. This example (white arrow) shows a rounded clast, but many also are angular. In size and shape, these resemble shards from weathered septarian concretions. (D) A rinded concretion cemented by iron oxide preserves bedding planes and a through-going joint.
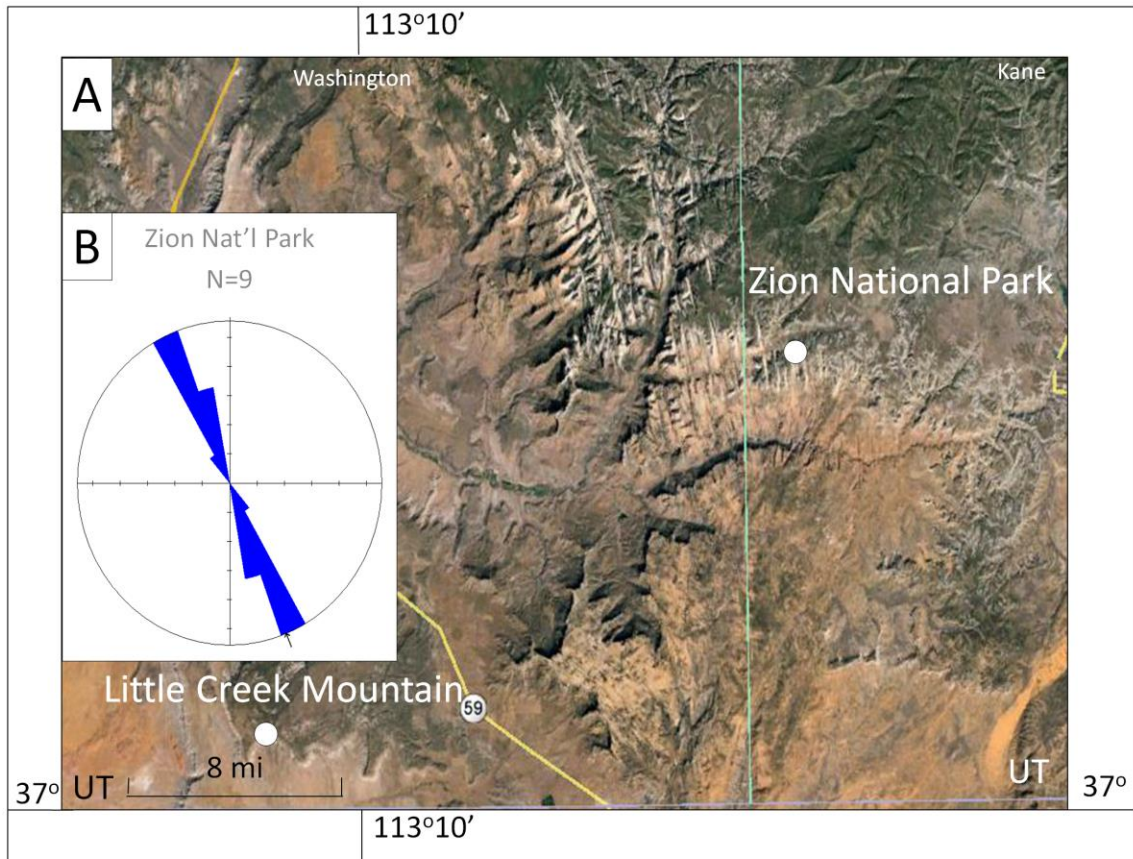
Figure 15: (A) Aerial photograph of Zion National Park where nine joint orientations (B) were measured. Joints strike 158°-338°. In plan view (C), iron-poor Shinarump outcrops similar jointing and patterns to those seen in iron-oxide box-work concretions. This photograph was taken at Shinarump Cliffs.
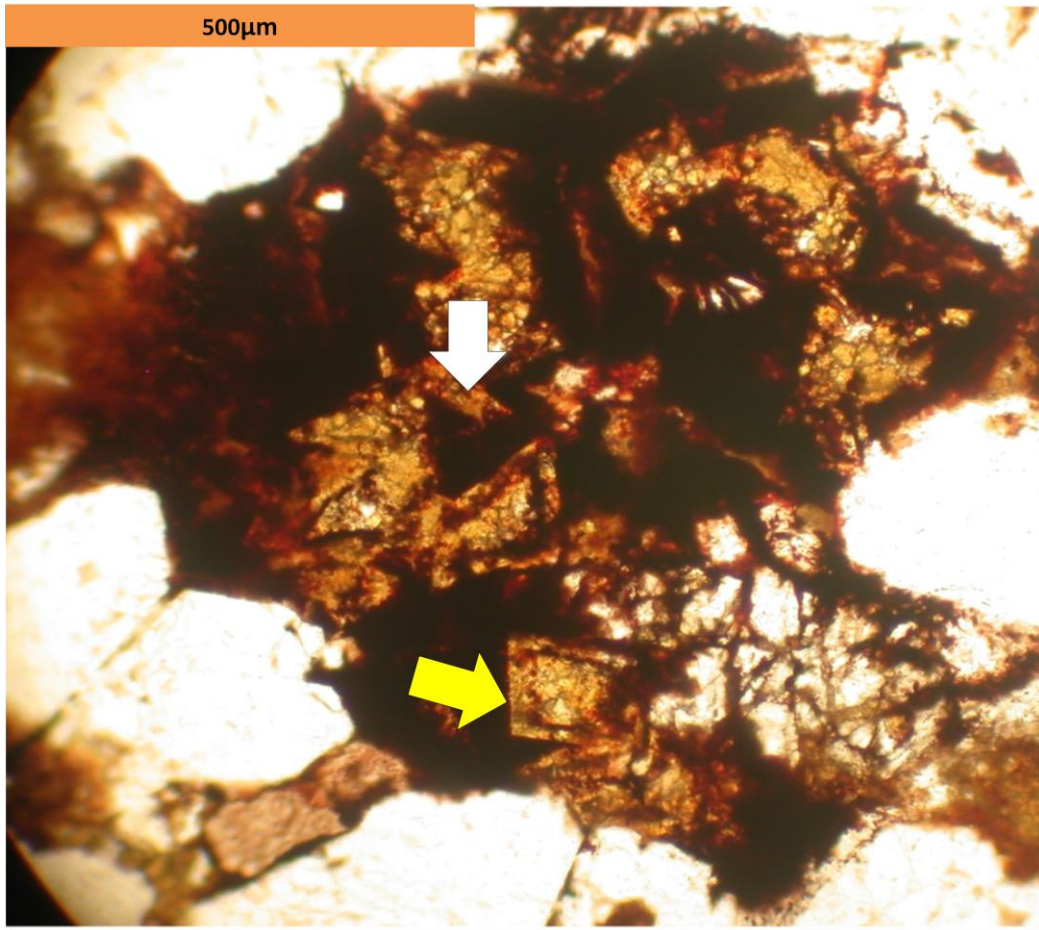
Figure 16: Thin-sections from Shinarump Cliffs of channel sandstones contain pore-filling siderite cement in channel sandstone (white arrow). When siderite oxidizes (yellow arrow) opaque iron-oxide cement forms along the rhombic cleavage planes. Siderite is readily oxidized in the presence of O_2. Siderite is actively being oxidized in the Shinarump Member.

Mineral Name	Area%
Quartz	63.83
K-feldspar	1.42
Plagioclase	0.14
Illite	7.22
Chlorite	0.74
Kaolinite	5.93
Calcite	1.31
Ankerite	0.13
Siderite	1.02
Phosphates	0.01
Ti Minerals	0.10
Pyrite	12.19
Fe Phase	5.30
Mn Phase	0.00
other minerals	0.56
Others	0.08

Figure 17: A thin-section of channel sandstones from Shinarump Cliffs was subjected to analysis by a QemScan microprobe and has produced a map of the mineral distribution across the thin-section. The minerals present are siderite (1%) and pyrite (more than 12%). Both of these minerals form anoxic, strong reducing waters.

1mm

are exposed and often eroded away. (Figure 11B) In some cases, dispersed iron-oxide cement is left in the center forming a less resistant core stone. Dispersed iron-oxide cement in core stones is not as densely cemented as rinds, but remains rigid when exposed. Upper and lower boundaries of box-works are less conspicuous than lateral boundaries formed by iron-oxide-cement around joints (Figure 14A). The upper boundary to box work concretions is the bedding contact between the thinly laminated mudstone and current rippled sandstone, but no iron oxide rind is found along this contact. The hatched pattern created by iron oxide cement around multiple joint sets is visible in many outcrops.

The current-rippled sandstone body has been cross-cut by more than one distinct fracture sets, and cemented by iron oxide that formed the eye-catching box-work concretions. In hand specimen, fractures associated with the box-work concretions penetrate on average ten centimeters below the thinly laminated mudstone into the current rippled sandstone body, but do not appear to disrupt any other beds. Fractures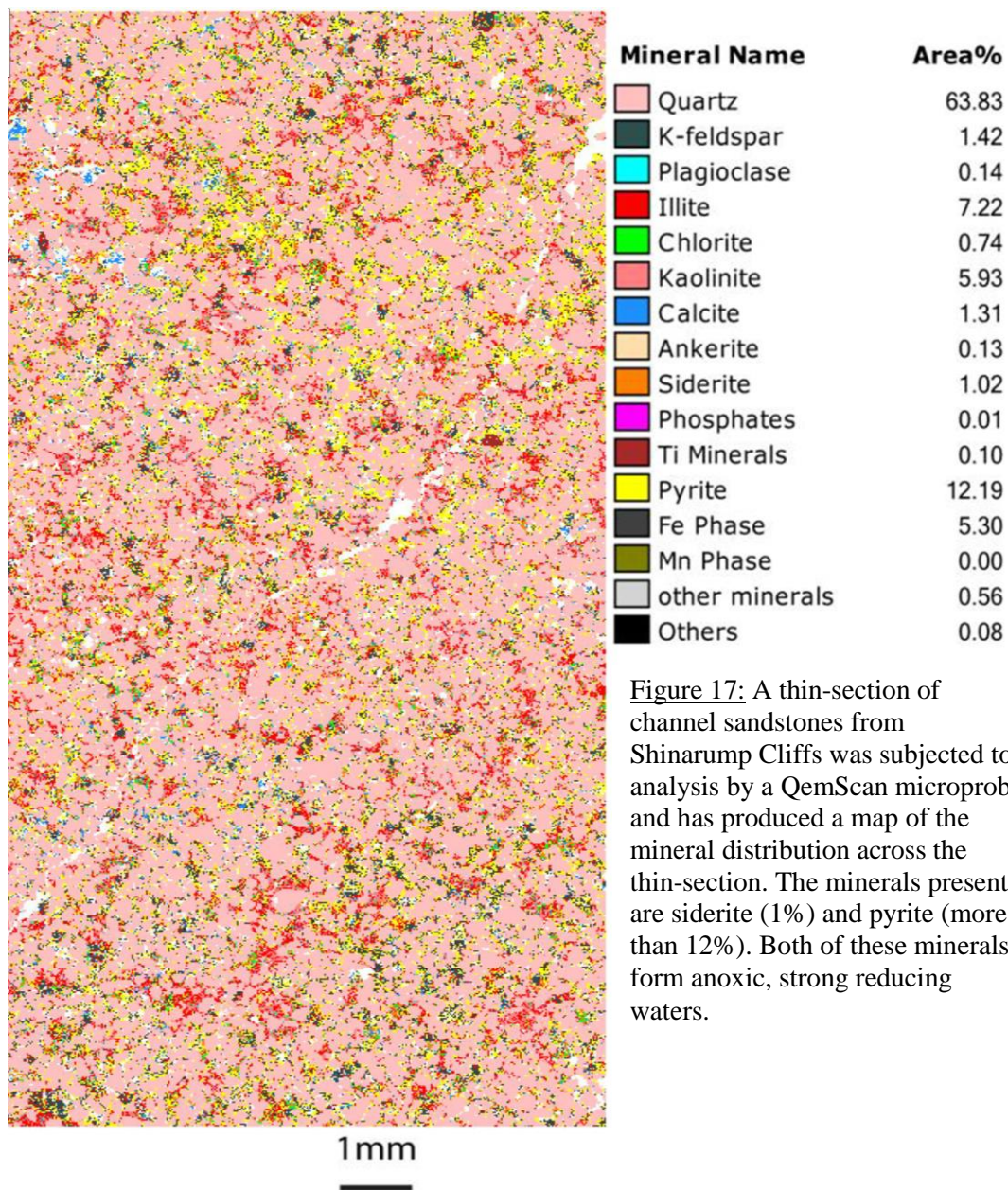 in the unit seem to penetrate to a common depth. Investigation via Google Earth and field work showed that the orientations of fractures in box-work concretions at Little Creek Mountain are parallel to the uncemented fractures occurring

Joints form the basic framework of box-work concretions. At the three study sites: 1) Little Creek Mountain, 2) Lost Spring Mountain, and 3) Zion National Park, we measured the orientations of joints. At Little Creek Mountain, 175 joint orientations were measured from box-work concretions (Figure 13C). At Lost Spring Mountain, some joints cut multiple rinded concretions. The orientations of six joints cutting through concretion rinds were measured and their mean resultant direction is $152^{\circ}/332^{\circ}$ (Figure 20A). Narrow canyons of Zion were formed by weathering along joints associated with Basin and Range faulting (Rogers et al., 2004). Nine orientations of the large joints at Zion National Park (Figure 15A) were measured; their mean resultant direction is oriented $158^{\circ}/338^{\circ}$ (Figure 15B).

i. Interpretation

The box-work concretions found in the Shinarump were initiated by early siderite (Figure 16) (Figure 17)cementation of the current rippled sandstone facies. Late diagenetic cementation by iron oxide along the contact between the thinly laminated mudstone and current rippled sandstone was localized by the previously existing siderite pore-filling-cement and the through-going joints. Microbes mediated the alteration of siderite to iron oxide.

The two main fracture sets cutting the Shinarump Member strike at 335° and 353°.The Shinarump joints measured at Little Creek Mountain and Lost Spring Mountain are parallel to Navajo Sandstone joints in Zion, indicating a regional joint pattern. According to Rogers et al. (2004), the joints in Zion formed during Miocene Basin and Range extensional faulting. Iron-oxide-cementation is also controlled by small-scale fracture sets. No joints were measured at the Shinarump Cliffs locality (Figure 15C), but the pattern displayed there by uncemented, cross-cutting joints has the same geometry and scale in outcrop as is seen in box-work concretions at Little Creek Mountain. The parallelism of the iron-oxide cemented joints in the Shinarump and large, open joints from nearby outcrops of the Navajo Sandstone indicate that iron-oxide cementation in the Shinarump post-dates Basin and Range faulting and fracturing.

In typical box-work concretions, iron-oxide rinds parallel joints. Iron for dense rinds likely originated as the reduced carbonate mineral siderite. Siderite was dissolved and the dissolved iron reprecipitated as iron-oxide-cement. Oxygen laden waters initially penetrated joints and prominent bedding planes. Oxidation took place along these planes and rinds formed along redox fronts controlled by iron oxidizing microbes. Rinds progressively thickened inwards towards dispersed, pore-filling rhombic siderite. Areas along joints and with less cement were the first to be oxidized. As oxidation progressed, rinds thickened, more siderite was dissolved and

more iron was oxidized. Oxidation was controlled by microbes and much of the original siderite was oxidized to make the rinds. If oxygen levels became too high, abiotic oxidation occurred leaving behind dispersed, pore-filling, and iron-oxide cements. (Figure 13B) The thick rinds found with typical box-work concretions suggest that microbes were able to stay in control of oxidation for relatively long periods of time.

      a. Horseshoe-Shaped Concretions

         i. Description

A second type of a box-work concretion (horseshoe-shaped) (Figure 13 C) was identified via a slabbed example. The slab has given useful insights that would not have ben possible by outcrop study alone. Unlike previously discussed box work concretions from the Shinarump Member and Navajo Sandstone examples, some iron oxide rinds do not immediately parallel fracture sets. The 'iron oxide rinds form horseshoe shapes instead maintain a similar pattern in plan view, but change considerably in vertical cross-section. Uncharacteristically, dispersed iron-oxide cement is found between iron-oxide rinds and joints (instead of rinds immediately adjacent to joints). Iron-oxide rinds that are several centimeters thick parallel fracture sets Rinds maintain a distance that is usually 2-3 centimeters from to the fracture (Figure 13D). Examination of fractures with a hand lens shows that they abruptly terminate, and that, near the depth of termination, rinds begin to curve toward the termination and finally join. Linking the two rinds creates a horse-shoe shaped rind that surrounds the joint, and surrounds the most densely cemented sediment. Areas outside of the rind are iron-poor in comparison. (Figure 13 C) The sandstone on the inside of the rind, including the joint fractures, contains dispersed iron oxide cement. Through further inspection of these box-work concretions, it became apparent that iron-oxide cementation is more complex. The bedding surface between the sandstone and the shale facies contains "failed rinds" that did not extend deeply into the sandstone to create a complete

Figure 18: Black spherical concretions in cross-bedded channel sandstones were cemented early. Photograph (A) reveals bedding planes diverting around the concretionary mass. (B) Rhombic-iron-oxide cement crystals are visible with the naked eye in channel sands and are interpreted as pseudomorphs after pore-filling siderite. (C) Rhombic-shaped, iron oxide masses in channel sands are interpreted as pseudomorphs after siderite. These two examples were oxidized abiotically and typify the cement within black spherical concretions.
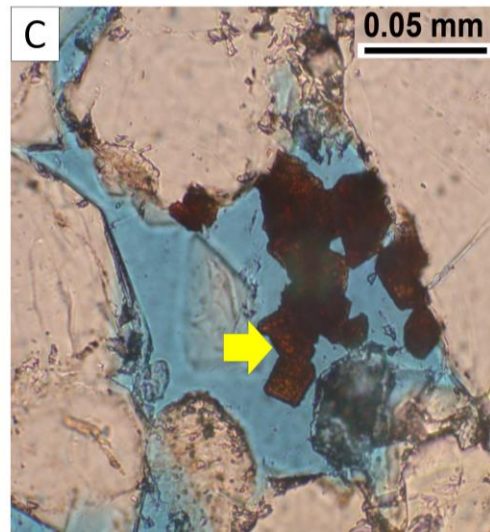
rind. Up to 2 or 3 of these failed rinds can parallel the complete rind. These incipient rinds, which are usually no more than a couple centimeters in length, dissipate into iron poor sediment. Inside these "failed rinds", toward the facture, dispersed iron oxide cement fills pore space between grains. This cement is not as dense as the cement inside the full horseshoe rind. These thin bands of iron oxide cement form irregularly located arcuate patches throughout box-work concretions.

ii. Interpretation

Horseshoe-shaped, box-work concretions are similar to the typical box works, but dispersed pore-filling cement is found around joints (Figure 13D), rather than directly adjacent to them. In comparison, these specimens have more bleached sandstone than areas with normal box-work concretions. Less cement allowed oxidation to happen faster before microbes were able to stabilize redox fronts and form iron-rich rinds. Because abiotic oxidation occurred first, dispersed iron-oxide-cement is found between rinds and joints. It is clear that once microbes were able to colonize these boundaries they controlled oxidation until it was complete. Little cementation took place along the contact between the mudstone and sandstone unit. The shale is highly impermeable, and the sandstone directly underneath was tightly cemented with pore filling siderite cement. Absence of avenues for groundwater flow likely explains the lack of an upper iron-oxide rind. Flow would have been through joints in the sandstone because evidence for abiotic oxidation along joints prior to rind formation indicates early oxidation. Rinds form because of the influence of microbes that stabilize redox fronts.

ii) Spheroidal Concretions

a. Black (Siderite)

i. Description

Although box-work concretions are more abundant, iron-rich, spheroidal concretions are
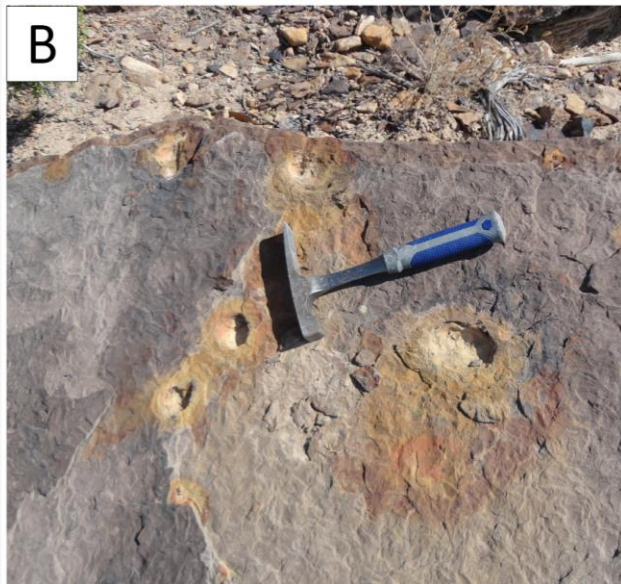
Figure 19: (A) Intact pyrite concretion is actively being oxidized in outcrop; iron oxide is actively precipitating around the concretion in channel sands. This is common because pyrite produces copious amounts of acid during oxidation causing ferric iron to mobilize and diffuse outward. (B) Concretions create voids as progresses.

also found within the channel sandstone facies (Figure 18A). Iron concretions are black in color because of evenly distributed iron-oxide-cement throughout the concretion (Figure 18 B, C). Grain size in the concretion is consistent with surrounding sediment. As bedding planes approach them, they are slightly diverted around the concretion. Like other concretions found in the Shinarump, some have fractures and others do not. Most fractures start and stop at the concretion edge, while others extend into adjacent sediment. Cementation is controlled by fractures starting and stopping at concretion edges, but fractures that extend into the adjacent sediment are not preferentially cemented.

i. Interpretation

Black spherical concretions display evidence for early cementation. Bedding planes are slightly deflected around black concretions indicating early cementation. Although channel sands do not compact much, differing amounts of cements can cause differences in volume causing bedding planes to be deflected. Although, preferential oxidation took place along some fractures penetrating concretion centers, not all of the cement was concentrated in rinds. Rinds have been cemented more densely than dispersed iron cement making up concretion interiors. It is probable that if thin-sections were made of these, rhombic iron-oxide pseudomorphs would be found as dispersed, pore-filling cement. No iron staining is present around edges of black spheroidal concretions (as opposed to the extensive stain around orange spheroidal concretions) (below). The black spheroids are tentatively interpreted as former siderite concretions that were abiotically oxidized.

a. Orange (Pyrite)

ii. Description

A second type of spheroidal concretion is typically smaller than the black concretions. Concretions do not follow joints or bedding planes. They are present in both the rippled sandstone and in the cross-bedded channel sandstone facies. Pyrite is visible in some of these concretions. Spheres are orange in color (Figure 21 A, B) and tend to hollow as they weather. Iron staining is prevalent and restricted to the area around the concretion. Staining from orange concretions can extend as vertical streaks down the face of the outcrop. No rinds form during the weathering process. Instead, streaking stains of Fe-oxide indicate active weathering of orange spheroidal pyrite concretions. Empty spheres are found in outcrop with box-work concretions. Spheres within box-work concretions do not have rinds and no iron staining is present in the surrounding rocks because it is heavily cemented by black iron-oxide cement.

iii. Interpretation

Orange staining around hollowed concretions in channel sands are the remnants of pyrite cement, as has been identified from outcrop examples. Pyrite has been identified by a microprobe scan of a thin-section, visually in outcrops, and via reflected light microscopy. Thin-sections were made from the channel sandstone facies and the thinly laminated mudstone unit that overlies the channel sandstone facies. Pyrite was found: 1) during examination of thin-sections, 2) as crystals visible by the naked eye from large discoidal septarian concretions, and 3) as dispersed cement in channel sandstone facies via microprobe analysis. As discussed earlier, pyrite is another mineral indicative of strong reducing conditions. Although pyrite and siderite do not commonly precipitate under the same conditions (Berner, 1981), it is not uncommon to find the two minerals in the same environment as conditions can change. With continued, heavy weathering, concretions become completely hollow. All that is left is iron staining around the concretion.
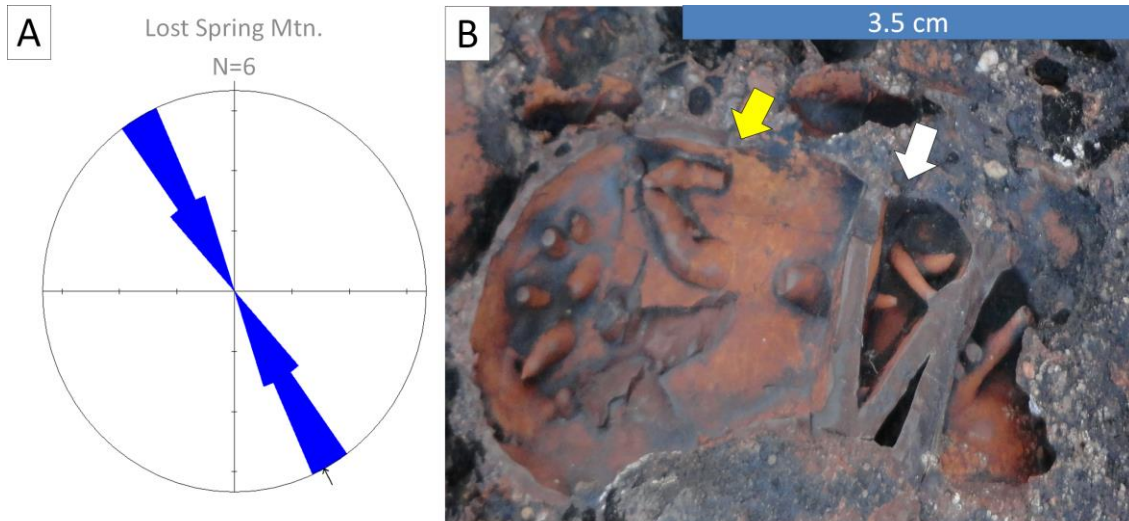
Figure 20: Orientations of joints in *in situ* concretions (A) at Lost Spring Mountain strike 152°-332°. (B) Tabular concretion displaying many tubular structures (yellow arrow) and through-going joints (white arrow). (C) Rinded tabular concretion displays wedge-shaped iron oxide fracture fills (white arrow) and botryoids (yellow arrow) on the concretion's inner rind. (D) Tabular concretion exhibits jointing on a small scale. Double wall of iron oxide cement bounds through-going joints. Joint orientations across the study area are parallel with joints having a Basin and Range origin (see Rogers et al., 2004).
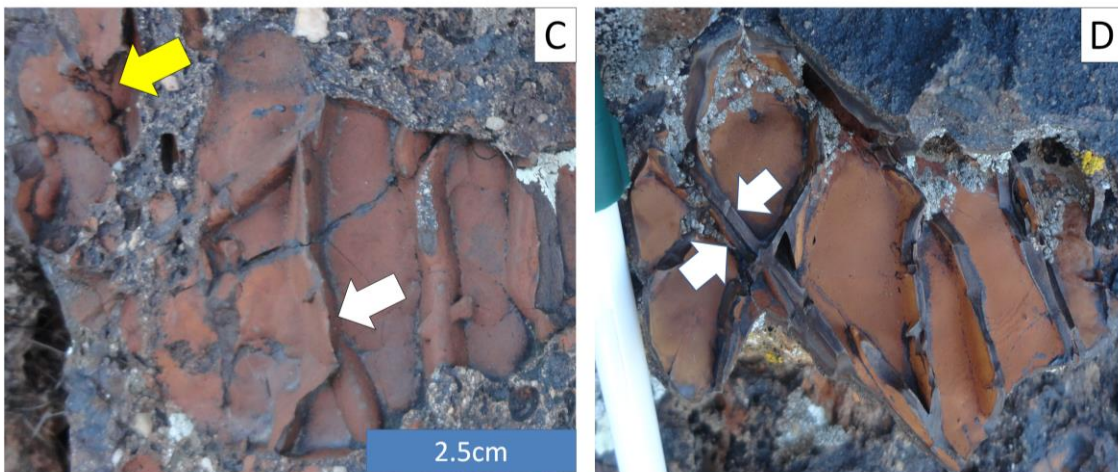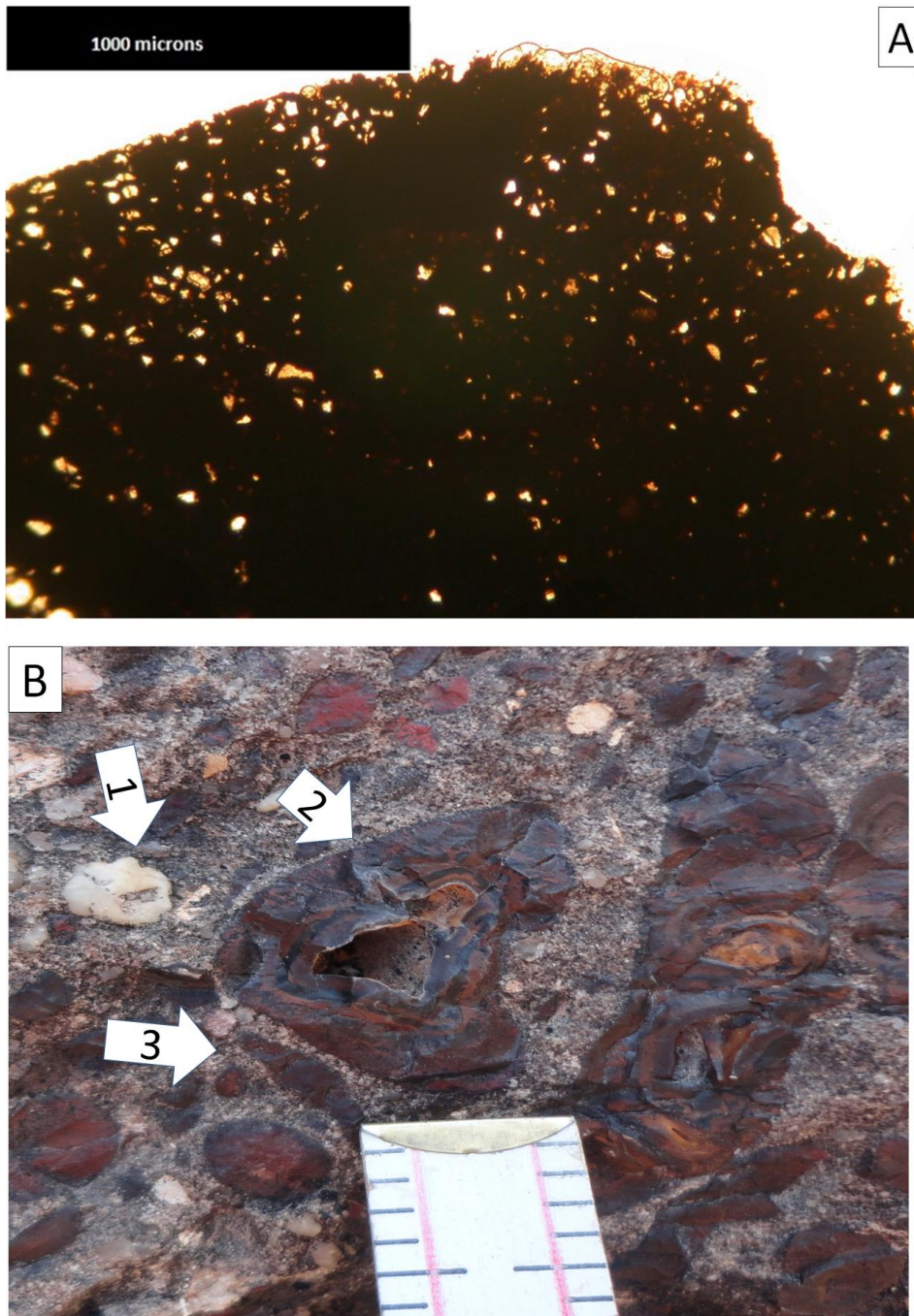
Figure 21: (A) Thin section of a concretion rind preserves evidence of previously existing pedogenic sphaerosiderite that originates in methanic flood plain deposits. Circular outlines are formed when radial displacive growth of siderite displaces silt and clay-sized quartz grains. The conglomerate in photograph (B) contains a variety of clasts: (B1) Chert an extrafromational conglomerate clast, (B2) rinded mudstone concretion with an unlithified, iron poor core, (B3) angular mudstone clast. Large tick mark on the scale marks 0.5 inches.

concretion. Due to the different modern oxidation processes observed associated with these pyrite concretions, it is evident that pyrite is not the precursor mineral for the previously discussed iron oxide concretions we see in outcrop.

Iron-Oxide-Cemented Conglomeratic Clasts

    i) *Rinded Concretions*

        a. *Description*

Iron-oxide-rich pebbles in Shinarump conglomerates are of two principle types. The first type of iron-oxide clasts is similar to the rinded concretions described by Loope et al., (2012) and Van der Burg (1969, 1970). They consist of a densely cemented iron-oxide rind, and an iron-poor center. Concretion centers in the Shinarump are either partially or completely empty because all rinded concretions found in outcrop were fragmented (Figure 20 B, C, D) allowing unlithified nucleus material to be eroded away. Few concretions in outcrop contain core material, but where present, it is composed of siltstone with an off-white color. Iron cemented sediment found in the core is usually rigid, dark in color, and fills a majority of the concretion interior. Cemented core material is less dense than iron-rich rinds. Shinarump rinded concretions are most commonly tabular in cross section, consistent with an origin as rip-up clasts. Other rinded concretions are irregular, ovoid, or spindle shaped.

Because iron-oxide minerals are opaque in thin section, other minerals that are found cemented together by iron oxide are easy to see. Clay and silt sized quartz clasts cemented by iron-oxide form distinctive patterns (Figure 21A). Typically, circular outlines are found. When outlines are densely populated or are touching, circles have been deformed (Figure 21A). Channel sandstone sediment is much coarser than the quartz grains that lie within the opaque iron-cement. A sharp contact exists between the opaque iron-oxide rinds (Figure 2BB) and material of the

concretion center. Uncemented core sediment is fine grained (silt and clay) and light grey,

whereas cemented sediment is dark in color.

Rinds display many associated features that are preserved by iron-oxide cementation. Fractures (Figure 20 B, C, D; Figure 14 D) associated with iron-oxide rinds are parallel with larger scale joints in outcrop. At Lost Spring Mountain, fractures in rinded concretions (Figure 20D) have a mean resultant direction of 152°-332° (Figure 20A). Joint fractures extending through the rinded clasts are enclosed by a double wall of iron oxide, one rind on each side of the fracture. When clasts are jointed, joints segment concretions into compartments. Wedge shaped, iron-cemented cracks (Figure 20C) have a different origin. They protrude inward toward concretion interiors, but do not cross cut entire concretions. They are neither parallel nor straight-edged but are irregular. Interior surfaces have sub-parallel ridges and tubes cemented by iron-oxide. Sub-parallel ridges found on interior surfaces of rinds merge and diverge from one another (Figure 14D). Tubes (Figure 20B) are found within concretion walls. Tubes protrude inward, curve, abruptly end (as if broken off), or taper in diameter and disappear. Although no tubes have been seen penetrating through entire concretions, it is probable that iron tubes extended through some concretions. Botryoidal texture (Figure 20C) is seen on some concretion interior surfaces.

a. *Interpretation*

Shinarump rinded concretions share three features with rattle stones from the Dutch Pleistocene: 1) bedding planes (Figure 5A), 2) botryoidal texture (Figure 5B), and 3) desiccation cracks (Figure 5C). The share three similar features with Dakota rattle stones: 1) jointed concretions (Figure 3A), 2) transported concretions (Figure 3B), and 3) circular outlines composed of quartz crystals (Figure 3C). Growth of sphaerosiderite crystals from the Dakota Formation (Figure 3D) provide an explanation for the circular outlines that are also present in the

Shinarump concretions. Similar cracks, textures, outlines, and grain sizes are found among all these concretions, indicating a similar origin.

The origin of the rinded concretions in Shinarump conglomerates is very similar to the origin of the rattle stone concretions in the Dakota Formation (Loope et al., 2012) and the Dutch Pleistocene (Van den Burg. 1969, 1970). Like their counterparts in younger strata, the Shinarump concretions take on the shapes of rip-up clasts and are often found in lag deposits. This explains why the grain size within rinded concretions is finer than that of fluvial sediment found in Shinarump channels (rip up clasts were derived from excised floodplain facies). Dense, thick rinds, structurally related, through-going fractures, and wedge shaped cracks can be found in all rinded concretions. In each of the three examples, oxidation along these planes was most likely controlled by iron-oxidizing microbes that occupied the redox fronts around concretions edges. Considering that cementation post-dates joint-related fractures, this indicates that oxidation of Shinarump rinded concretions was much later than the Triassic, and no earlier than the onset of Basin and Range deformation. Shinarump rinded concretions have wedge-shaped cracks, most likely formed during the short transport of mudstone clasts from the flood plain facies. Some cracks may have formed during transport of the mudstone clasts down fluvial channels. Mudstone clasts were likely abraded and then exposed on sand bars or banks to dry, forming desiccation cracks. Evidence from concretion rinds points towards a floodplain origin, as the inside surface of concretion rinds presents fine linear ridges that join and diverge. These ridges are mostly likely zones of increased iron cementation which occurred along bedding planes. An inner botryoidal texture is found on the inner surfaces of concretions from both the Dutch Pleistocene and from the Shinarump, and may relate to the configuration of microbial colonies. Tubular structures in the Shinarump, like those in the Dakota, are the size and shape of roots traces. Iron oxide rinds also present evidence indicative of a water-logged floodplain facies. Circular outlines formed by

silt-sized to very-fine quartz grains provide evidence of displacive mineral growth. Quartz grains were displaced by sphaerosiderite crystals in shallow, water-logged, organic rich, and methanic conditions in fluvial floodplain facies. Because many of the same features are shared between the rinded concretions in the Shinarump as the previously studied rattle stones, we can call Shinarump rinded-concretions rattle stones (even though they do not produce the audible rattling sound that is heard from other concretions).

    i)   *Iron-oxide-cemented Clasts*

          a.   *Description*

The second type of intraformational iron-oxide clasts found in Shinarump conglomerates does not have the iron-rich rinds and iron-poor centers that characterize rinded concretions. Instead, these reworked clasts are composed of rounded, angular, tabular, curved and irregular shaped conglomeratic pebbles consisting of both mudstone (Figure 14C and 21B) and sandstone (Figure 14B). Pebbles are evenly cemented throughout instead of preferentially cemented around joints or the perimeters of clasts. They bear no joints or other signs of deformation. Sandstone clasts have iron oxide speckles indicating dispersed, pore-filling, iron-oxide cement. Some mudstone clasts display dendrites.

          b.   *Interpretation*

Unlike the rinded concretions that have fractures parallel to outcrop-scale joints indicating timing of oxidation, it is not clear whether these unjointed and unrinded clasts have been oxidized during early or during late diagenesis. It is likely some oxidation took place early, because reduced iron minerals in the clasts would have been exposed to highly oxygenated, turbulent conditions during transport in the Triassic streams. If the siderite cemented mudstone

clasts were only partially oxidized during deposition, the oxides would likely form only a thin crust of iron oxide, and not evenly cement the entire concretion. These likely would have been subjected to the same fate as other mudstone clasts found within the Shinarump (oxidation with rind formation). Because no rind is formed and the first exposure to oxidizing system was likely during transport of these clasts, they were probably oxidized abiotically in the depositional environment.

Unrinded clasts that are angular and curved have similar shapes as the modern clasts derived from shattered, oxidized (ancient) iron-oxide concretions exposed in modern outcrops of the thinly laminated mudstone unit. This further suggests that at least some conglomeratic clasts were oxidized either before or during stream transport and redeposited as lags. This evidence, like that from the other concretions, is consistent with early diagenetic siderite. Further investigation is needed to help determine timing of oxidation. One method for dating iron oxides is to use helium-thorium-uranium dating (Reiners et al., 2013).

DISCUSSION & CONCLUSION

Discoidal septarian concretions occur in a thinly laminated mudstone facies above channel sandstone and displays complex fracture networks, iron oxide cement, and abundant siderite cements. Rattle stones, iron-oxide pebbles, cemented channel sands, and septarian concretions provide valuable information about Shinarump floodplain hydrology and its diagenetic history. Understanding these early diagenetic iron accumulations found within the Shinarump Member of the Chinle Formation are vital to understanding its depositional environment and diagenesis. Iron-rich concretions have the appearance of iron-oxide in both outcrop and thin-section, but some retain the unoxidized reduced iron minerals siderite, rhodochrosite, and pyrite. Reduced iron minerals have been identified using traditional microscopes and by analysis using QemScan (microprobe). The reduced iron carbonate minerals

are indicative of strongly reducing sediments that are rich in organic matter and generally poor in sulfate. Analogous environments are found associated with a high groundwater table and methanic conditions in modern freshwater swamps and bogs. Not only have iron-oxide-cements and iron-oxide cemented clasts been found in all facies, but siderite has been found in the thinly laminated mudstone in septarian concretions and as dispersed pore-filling cement in the channel sandstone facies. The rinds on transported clasts contain evidence for displaced silt and clay attributable to the growth of sphaerosiderite crystals that are found in abundant in both modern and ancient flood plain deposits. Dispersed rhombic siderite in channel sandstone facies was the source of iron for iron-oxide-cemented spheres, boxes and the wonderstone. Perhaps the most significant conclusion of this study is that although there is abundant evidence for an early (Triassic) origin for the ferrous iron minerals in the Shinarump, there is also abundant evidence that the bulk of this iron was not oxidized to ferric phases until the Colorado Plateau was uplifted in the Neogene. This conclusion is supported by the fact that cementation is preferential along joints-- joints aided in the oxidation of early diagenetic siderite in both the box-work and the rinded concretions. Joint orientations are consistent across the study area including joints found in the Navajo Sandstone that have been linked to Basin and Range extension. Oxygen laden, meteoric waters were able to penetrate all joints sets as the Colorado Plateau was uplifted. Joints provided optimal habitats for iron oxidizing microbes. Rinds along joints grew as dissolved iron diffused towards the redox front where iron oxidizing microbes were able to metabolize the ferrous iron and to ferric iron.

REFERENCES

Beer, J. J., University of Minnesota, Duluth: 2005. Sequence stratigraphy of fluvial and lacustrine deposits in the lower part of the Chinle Formation, south central Utah, United States: paleoclimatic and tectonic implications (M.S. thesis).

Beitler, B., Chan, M.A., and Parry, W.T., 2003, Bleaching of Jurassic Navajo Sandstone on Colorado Plateau Laramide highs: Evidence of exhumed hydrocarbon supergiants?: Geology, v. 31, p. 1041– 1044.

Berner, R.A., 1981, A new geochemical classification of sedimentary environments: Journal of Sedimentary Petrology, v.51, p.359-365.

Blakey, R.C., Gubitosa, R., 1983, Late Triassic paleogeography and depositional history of the Chinle Formation, southeastern Utah and northern Arizona. *In*: Reynolds, R. M. and Dolly, E. D., eds., Mesozoic paleogeography of west-central United States. Rocky Mountain Section, Society of Economic Paleontologists and Mineralogists, Denver, Colorado, p.57-76.

Chan, M.A., Johnson, C.M., Beard, B.L., Bowman, J.R., Parry, W.T., 2006, Iron isotopes constrain the pathways and formation mechanisms of terrestrial oxide concretions: A tool for tracing iron cycling on Mars: Geosphere, v. 2, no. 7, p. 324-332.

Chan, M.A., Bowen, B.B., and Parry, W.T., 2005, Red rock and red planet diagenesis: Comparisons of Earth and Mars concretions: GSA Today, v. 15, no. 8.

Chan, M.A., Bowen, B.B. and Parry, W.T.,(2004) A Possible terrestrial analogue for hematite concretions on Mars: Nature, v.429, p. 731-734.

Curtis, C. D., and Coleman, M. L. 1986. Controls on the precipitation of early diagenetic calcite, dolomite, and siderite concretions in complex depositional sequences. *In* Gautier, D. L., ed. Roles of organic matter in sediment diagenesis. SEPM Spec. Publ. 38, p. 23–33.

Dickinson, W. R., 1981, Plate tectonic evolution of the southern Cordillera, *In* Dickinson, W., R., and Payne, W.D., eds., Relations of Tectonics to Ore Deposits in the Southern Cordillera: Arizona Geological Society Digest, v. 14, p. 113-135.

Dickinson W.R., Gehrels, G.E., 2008, U-PB Ages of detrital zircons in relation to paleogeography: Triassic Paleodrainage networks and sediment dispersal across southwest Laurentia: Journal of Sedimentary Research, v.78, p.745-764.

Dubiel, R.F., and Hasiotis, S. T., 2011, Deposystems, paleosols, and climatic variability in a continental system: the upper Triassic Chinle Formation, Colorado Plateau, U.S.A.: *In* Davidson, S.K., Leleu, S., and North, C.P. (eds.) The Preservation of Fluvial Sediments and Their Subsequent Interpretation, Edition: SEPM Special Publication No. 97, , p.393–421

Dubiel, R.F., Parrish, J.T., Parrish, J.M., Good, S. C., 1991, The Pangaean Megamonsoon-Evidence from the Upper Triassic Chinle Formation, Colorado Plateau: Palaios, v.6, p.347-370.

Hintze, L.F., 1988, Geologic History of Utah: Provo:*In* Kowallis, B.J. (ed.), Brigham Young University Geology Studies Special Publication 9, 202 p.

Ho, C. and Coleman, J.M. (1969) Consolidation and cementation of recent sediments in the Atchafalaya basin. GSA Bull., v. 80, p. 183–192.

Kettler, Richard M., Loope, David B., Niles, Paul B., and Weber, Karrie A., 2012, Geochemical self-organization and microbially-mediated oxidation of siderite in the Shinarump Member of the Chinle Formation: Geological Society of America Abstracts with Programs, Vol. 44, No. 7, p. 363.

Kutzbach, J. E., and Gallimorre, G., 1989, Pangaean climates: Megamonsoons of the megacontinent: Journal of Geophysical Research, v. 94, p. 3341-3357.

Loope, D.B. Kettler, R.M., Weber, K.A., 2010, Follow the water: Connecting a CO_2 reservoir and bleached sandstone to iron-rich concretions in the Navajo Sandstone of south-central Utah, USA: Geology, v.38, no. 11, p. 999-1002.

Loope, D.B. Kettler, R.M., and Weber, K.A., 2011, Morphologic Clues to the Origins of Iron Oxide–Cemented Spheroids, Boxworks, and Pipelike Concretions, Navajo Sandstone of South-Central Utah, U.S.A.: Journal of Geology, v.119, p. 505-520.

Loope, D.B. Kettler, R.M., Weber, K.A., Hinrichs, N.L., and Burgess, D.T., 2012, Rinded iron-oxide concretions: hallmarks of altered siderite masses of both early and late diagenetic origin: Sedimentology, v. 59, p. 1769-1781

Ludvigson, G.A., Gonzalez, L.A., Metzger, R.A., Witzke, B.J., Brenner, R.L., Murillo, A.P., and

White, T.S., 1998, Meteoric sphaerosiderite lines and their use for paleohydrology and paleoclimatology: Geology, v.26, p. 1039-1042.

Ludvigson, G.A., and Ravn, R.L., 1996, New Insights on the Sequence Stratigraphic Architecture of the Dakota Formation in Kansas-Nebraska-Iowa from a decade of sponsored research activity: Current Research in Earth Sciences, Bulletin 258 p. 1039-1042.

Mozley, P.S., and Carothers, W.W., 1994, Elemental and Isotopic Composition of Siderite in the Kuparuk Formation, Alaska: Effect of Microbial activity and water/sediment interaction on early pore-water chemistry: Journal of Sedimentary Petrology, v.62, p. 681-692.

Melezhik, V.A., Fallick, A.E., Smith, R.A., and Rosses D.M., 2007, Spherical and columnar, septarian, 18O-depleted, calcite concretions from Middle-Upper Permian lacustrine siltstones in northern Mozambique: evidence for very early diagenesis and multiple fluids: Sedimentology, v.54, p.1389-1416.

Mortimer R.J.G., Galsworthy, A.M.J, Bottrell, S.H., Wilmot, L.E., and Newton, R.J., 2011, Experimental evidence for rapid biotic and abiotic reduction of Fe (III) at low temperatures in salt marsh sediments: a possible mechanism for formation of modern sedimentary siderite concretions: Sedimentology, v.58, p.1514-1529.

Mozley, P.S., 1996, The internal structure of carbonate concretions in mudrocks: a critical evaluation of the conventional concentric model of concretion growth: Sedimentary Geology, v.103, p.85-91.

Mozley, P.S., 1989, Relation between depositional environment and the elemental composition of early diagenetic siderite: Sedimentary Geology, v.17, p.704-706.

Parrish, J.T., 1985, Latitudinal distribution of land and shelf and absorbed radiation during the Phanerozoic: U.S. Geological Survey, Open-File Report 85-31, 21 p.

Peterson, F., 1988, Pennsylvanian to Jurassic eolian transportation systems in the western United States: Sedimentary Geology, v.56, p. 207-260.

Pratt, B.R., 2001, Septarian concretions: internal cracking caused by synsedimentary earthquakes: Sedimentology, v.48, p.189-213.

Prochnow, S. J., Nordt, L.C., Atchley S.C., and Hudec, M.R., 2006, Multi-proxy paleosol evidence for middle and late Triassic climate trends in eastern Utah. Palaeogeography, Palaeoclimatology, Palaeoecology, v. 232, p. 53– 72

Pye, K., Dickson, J.A.D., Schiavon, N., Coleman, M.L., and Cox, M., 1990, Formation of Siderite-Mg-calcite-iron sulphide concretions in intertidal marsh and sandflat sediments, north Norfolk, England: Sedimentology, v.37, p.325-343.

Reiners, P. W., Chan M. A., and Evenson N., 2013, (U-Th)/He dating and chemistry of diagenetic Fe-Mn-oxides in Mesozoic sandstones of the Colorado Plateau. Abstract, AGU Annual Meeting, San Francisco, Control ID 1788975.

Rogers, C. M., Douglas, A.M., and Engelder T., 2004 Kinematic implications of joint zones and isolated joints in the Navajo Sandstone at Zion National Park, Utah: Evidence for Cordilleran relaxation. Tectonics, v. 23, TC1007, doi: 10.1029/2001TC001329.

Stewart, J.H., Poole, F.G., and Wilson, R.F., 1972, Stratigraphy and origin of the Chinle Formation and related Upper Triassic strata in the Colorado Plateau region: U.S. Geol. Survey Prof. Paper 690, 336.

Ufnar, D.F., Gonzalez, L.A., Ludvigson, G.A., Brenner, R.L., Witzke, B.J., and Leckie, D., 2005, Reconstructing a Mid-Cretaceous Landscape from Paleosols in western Canada: Journal of Sedimentary Research, v.75, p. 984-996.

Van der Burg, W.J., 1969, The formation of rattle stones and the climatological factors which limited their distribution in the Dutch Pleistocene, 1.The formation of rattle stones: Paleogeography, Paleoclimatology, Paleoecology, v.6, p.105-124.

Van der Burg, W.J., 1970, The formation of rattle stones and the climatological factors which limited their distribution in the Dutch Pleistocene, 2. The climatological factors: Palaeogeography, Palaeoclimatology, Palaeoecology, v.6, p. 297-308.

Weber, K.A., Spanbauer, T.L., Wacey, D. Kilburn, M.R., Loope, D.B., Kettler, R.M., 2012, Biosignatures link microorganisms to iron mineralization in a paleoaquifer: Geology, v.40, p. 747-750.

Ziegler, A.M., Scotese, C.R., and Barrett, S.F., 1982, Mesozoic and Cenozoic Paleogeographic

maps. *In* Broshe, P. and Sundermann, eds., Tidal Friction and the Earth Rotation, Springer-Verlag, Heidelberg, p. 240–252.